UNIVERSIDADE DE LISBOA
FACULDADE DE CIÊNCIAS
DEPARTAMENTO DE FÍSICA

Phase diagrams of linker-monomer binary mixtures: effects of size and gravity.

Rodrigo Braz Teixeira

Mestrado em Física

Especialização em Física Estatística e da Matéria Condensada

Dissertação orientada por:
Prof. Dr. José Maria Tavares
Prof. Dr. Margarida Telo da Gama

2020

Abstract

Colloids are mesoscopic particles, each about a few hundred nanometers in size, dispersed in a fluid. While natural colloids are ubiquitous in nature, from clouds to food, synthetic colloids with well-controlled size distributions and interactions can be synthesized in the lab. Colloids form crystals, liquids, and other phases of matter also observed in atomic and molecular systems, making them excellent candidates to study phase transitions both theoretically and experimentally. Patchy colloids are the epitome of such particles. They are part of a generation of colloidal particles that break orientational isotropy with designed patches on their surface through which colloidal particles can self-assemble. Diverse applications have already been developed, from photonic crystals to drug delivery systems. Here, we study the phase behavior of a binary mixture of patchy colloids using Wertheim's first order perturbation theory and Tavares et al. generalization of Stockmayer's random bond percolation theory. We also analyze the effect of changing the relative size between the different species and, using de las Heras et al. sedimentation theory, the effect that gravity has in the system is also considered. Our main results show a complex phase behavior with two different topologies depending on the thermodynamic parameters such as pressure and temperature. A rich phase stacking phenomenology is observed in sedimentation-diffusion-equilibrium, with more than twenty different stacking sequences and up to five different stacks in a single sequence.
Keywords: Patchy colloids, binary mixture, phase behavior, sedimentation.

Resumo

Colóides são partículas nanométricas dispersas num fluido. Na natureza estas misturas encontram-se em diversos materiais, desde as nuvens à comida, e são responsáveis por fenómenos como o efeito de Tyndall. No entanto, são os colóides artificiais (criados em laboratório) com interações e distribuições de tamanho desenhadas à medida que têm sido investigadas e instigado maior interesse na comunidade cientifica, em particular estas partículas tem sido utilizadas como modelos para melhor compreender transições de fase: Por um lado, estas partículas podem formar fases semelhantes às observadas em sistemas moleculares e atómicos, servindo como modelo para aceder a estas transições normalmente inacessiveis experimentalmente. Por outro lado, estes sistemas têm interesse por si só, demonstrando comportamento coletivo complexo sem comparação em sistemas atómicos. Colóides *patchy* são o epitome destas partículas, fazendo parte de uma geração de colóides anisotrópicos devido aos *patches* construídos na sua superfície por onde podem ser feitas as ligações entre partículas. Existem já diversas aplicações desenvolvidas com estas partículas, desde cristais fotónicos a sistemas de administração de medicamentos. Devido às suas dimensões, numa experiência com colóides, a presença de efeitos gravitacionais é frequentemente inevitável. Por isso, a sedimentação (a progressiva deposição de partículas num fluído) é uma ferramenta para estudar diversas propriedades destas misturas. Desde o cálculo da equação de estado à determinação da constante de Boltzmann. Para além de servir como uma ferramenta, a sedimentação de colóides *patchy* tem demonstrado resultados interessantes, como fases mais densas presas entre fases menos densas.

Neste trabalho, considera-se uma mistura binária de colóides *patchy* com um número diferente de *patches* de diferentes espécies. Particularmente, é estudado o caso em que uma das espécies tem 2 *patches* (2A) e a outra 3 *patches* (3B). Somente a ligação entre partículas de diferentes espécies é permitida. Desta forma, uma escala de energia, ε, que caracteriza a ligação entre as partículas é definida e a quantidade de ligações entre parículas de uma espécie passa a ser controlável através da composição da outra. É investigado o comportamento de fase em volume deste sistema, a sua dependência na temperatura e na pressão, e o efeito de alterar o tamanho relativo das partículas. Também é estudada a fenomonologia de pôr o sistema sobre gravidade, é considerado o caso em que as amostras têm um comprimento infinito. É calculado o *stacking diagram* que permite saber quais as sequências que se podem obter assim que o equilibrio é estabelecido, e para que parâmetros do sistema se obtém cada sequência de fases.

O comportamento de fase é estudado através da teoria perturbativa de Wertheim e da generalização da teoria de percolação *random bond* de Stockmayer por Tavares *et al.*.Utilizando a teoria de sedimentação por de las Heras *et al.* o efeito de colocar o sistema sob gravidade é considerado. Os nossos resultados principais demonstram um comportamento de fase complexo. O diagrama de fases apresenta duas topologias diferentes dependendo dos valores de temperatura e pressão: uma apresentando duas regiões de coexistência, uma abundante em partículas 2A e outra em 3B. Entre as regiões encontra-se um ponto azeotrópico e fechando cada região um ponto crítico inferior. A segunda topologia consiste num hiato de

miscibilidade na região abundante em partículas 3B com um ponto crítico inferior e outro superior. As linhas de percolação demonstram a percolação da fase menos densa, sendo que a fase mais densa se encontra sempre percolada. O estudo da sedimentação demonstrou que para a primeira topologia, obteve-se mais de vinte sequências de fases. Para a segunda obteve-se cinco sequências. Ainda se mostrou que as misturas com partículas de tamanhos diferentes não formaram diferentes topologias e que o efeito de alterar o tamanho podia ser aproximado ao efeito de alterar a temperatura e a pressão. Por fim, mostrou-se que é possível alterar as sequências de sedimentação ao alterar o tamanho das partículas.
Palavras-chave: Colóides, partículas *patchy*, mistura binária, sedimentação, comportamento de fase.

Acknowledgments

First, I would like to thank the professors, without their help this work wouldn't exist. José Maria Tavares was always available and patient for every question imaginable. Daniel de las Heras always guided me in the right path, predicting and preempting the problems I would encounter. Margarida Telo da Gama taught my first Physics university class and made me believe I was in the right place. All this traces back to Nuno Araújo who was always an inspiration and helped me figure out where to go in multiple occasions. I would like to thank my family, who had one of the hardest tasks - making sure I ate enough food and drank enough water. And finally, thank you to those who slowed me down, dragged me out of the house and got me out of my head: Beatriz, Martim, Filipe, João, André, Marchana, Rita, Maria, Joana, Mariana, Gerson and Jessica.

Index

List of Figures

Chapter 1

Introduction

1.1 General framework

Statistical Physics provides a bridge between the microscopic and the macroscopic world. This approach follows from the understanding that matter is composed of many constituents such as e.g. electrons, atoms and molecules. This means that the trajectories of individual constituents cannot be followed. Instead, averages of characteristic properties through some sort of statistical treatment must be used [1]. This is where Statistical Mechanics comes in, extending Thermodynamics to a deeper understanding of matter by proposing to study the properties of macroscopic systems in equilibrium from the microscopic equations of motion. The recipe is to build the partition function, a function of the macroscopic parameters that counts the number of microstates and that relates to a thermodynamic potential and therefore to any thermodynamic variable [2]. In order to write the partition function, we need to know exactly the interactions between the particles and sum over all microstates of the system. For simple systems like the ideal gas, this can be done (see appendix 6.1). But for more complex and realistic situations, this approach is not feasible.

Phase transitions have consistently been among the principal subjects of active studies in statistical physics [3] and they are perfect examples of macroscopic phenomena explained in terms of its constituent's microscopic laws. The interest may arise from the fact that different phases of the same material usually mean different behaviour. Examples are everywhere, from the familiar three states of matter to exotic superconductors and liquid crystals. A thermodynamic system is characterized by a thermodynamic potential (e.g. the Helmholtz free energy) and each phase may be defined by imposing certain conditions to this potential (e.g. equality of the chemical potentials). The phase diagram is a representation of the stable phases of the system for a chosen set of variables. By using different variables of the thermodynamic potentials, it is possible to have different phase diagram representations that best suit each particular study. The basic strategy of theoretical studies of phase transitions is to find the phase diagram for the model under study. In some simple cases it is possible to derive exact solutions by sophisticated methods. However, in general, we have to resort to approximate and numerical methods to understand the essential features of the physical phenomena under consideration.

1.2 The colloidal realm

Colloids are solid or liquid particles, each about a few hundred nanometers in size, dispersed in a solvent and subject to thermal fluctuations. While natural colloids are present everywhere in nature - e.g. paint, milk, glue and blood - synthetic colloids with well controlled shapes, size distributions and interactions can also be synthesized. A feature of colloids that drives much current research is their collective behavior - their ability to self assemble into complex structures and their rich phase behavior. By exploring how these effects emerge, one gains insights into deeper questions like how matter organizes itself [4]. Applications are varied and diverse. Technological applications are, for example, photonic crystals [5] and conductive ink [6]. These applications make use of the fact that colloids can form regular structures on a lengthscale at which visible light is difracted. Structures on the colloidal lengthscale are also found in our bodies, making colloidal research vital for medical applications such as drug delivery [7]. Colloidal particles are generally large and slow enough to be observed via optical microscopy. For this reason, colloids are used to model and understand other systems. For example, the mechanisms of protein assembly that occur at the molecular lengthscale can be partially understood by studying colloidal systems [8]. Because colloidal systems can form crystals, liquids and other phases of matter that occur in atomic and molecular systems they have also been used to model these systems, allowing the understanding of the microscopic mechanisms of phase transitions [9].

Patchy particles are colloidal particles with designed patches on their surface displaying short range and highly directional interparticle forces. They are part of a generation of colloidal particles that break orientational isotropy. For these reasons, the phase behavior is potentially much richer than that of colloidal spheres; isotropy is an idealization and should be treated either as an approximation or as a zeroth-order point of departure for the analysis of more complex and realistic situations [10]. Examples of this rich phase behavior are empty liquids [11] (liquid states with a vanishing occupied packing fraction), network fluids (structured fluids consisting of chains and branches) with pinched phase behavior [12] and lower critical points [13]. Patchy particles have been used to model associating fluids [14], proteins [15], and are ever present in the mesoscopic domain of soft matter physics. There are different methods for synthesizing patchy colloids [16], from site-selective deposition on colloidal monolayers to seeded polymerization on colloidal clusters.

The phase behavior of these systems has been studied before. Two systematic studies of binary mixtures were done by de las Heras et al.. In [17], all bonding sites were identical (single energy scale and bonding probability) and the effect of the entropy of bonding was studied. It was found that the functionality (i.e. the number of patches per particle) was a key parameter in the phase behavior (controlling both the topology, the nature and number of fluid phases). In [18], mixtures of particles with 2 and 3 patches of different types were considered (this defined 3 energy scales) and the empty liquid regime was studied in depth. Simulation and experiments have also been performed for different systems. For example, in [11] the first simulations were performed and the concept of empty liquid was introduced. In [19] the effect of the functionality of the particles on the phase behaviour was experimentally verified.

In a colloidal experiment, the presence of gravitational effects is often unavoidable [20]. This is a reason why sedimentation (the progressive settling of particles in a fluid) [21], which in everyday life is relevant from blood analysis to the shelf life of paint, is a means to study the collective behaviour of colloidal mixtures. For example, by observing the distinct layers (or stacks) in samples that form in the sedimentation-diffusion equilibrium of a sample, the phase boundaries can be determined. However, disentangling the effects due to interparticle interactions, which generate the bulk phase diagram, from those due to gravity is a complex task [22]. De las Heras et. al. recently tackled this problem using a

theory that explicitly relates the bulk phase diagram to its phase stacking phenomenology under gravity through a local density approximation. This theory has been applied to patchy particle systems in [23, 24]. A rich phase stacking phenomenology was found, including the formation of multiple stacks and denser particles floating on top of lighter ones, both in the case of infinite (very high) and finite sample sizes [25].

In our work, we consider a binary mixture of patchy colloids with a different number of distinct bonding sites. Particularly we study the case where only inter-species bonding is allowed. This defines an energy scale, ε, which characterizes the bond between two particles. In this way we can control the extension of bonds of one species with the other (if we only have one species no bonding is allowed). Furthermore, we model the bonding interaction through square well potentials, in such a way that the bonding volume is constant throughout. We investigate the bulk phase behavior of this system, the dependence on temperature and pressure, and the effect of changing the relative size of the particles. We then study the phase stacking phenomenology of the system under gravity. We consider the case of infinite (very high) sample heights and calculate the stacking diagram (the set of all possible stacking sequences of different layers in colloidal mixtures due to sedimentation). The effect of changing the particle size is novel and both the effect of gravity and the phase behavior for this particular system have not been studied before. The structure of the thesis is as follows: In chapter **2** we present the particle model and lay out the theoretical basis to study the phase behavior; in chapter **3** the phase behavior results and the effect of changing the relative size of the particles is studied; and in chapter **4** the theoretical framework and results of putting both the equal size and different size systems under gravity is considered.

Chapter 2

Theoretical framework

The system under study is a binary mixture of patchy colloids. The particles are hard spheres (impenetrable spheres that cannot overlap in space) with diameter σ_i. The particle species is defined by the size of the particle and the number of patches $f_\alpha^{(i)}$ of type α on their surface, $i = \{1,2\}$, $\alpha = \{A,B\}$. The pair potential between particles i and j is given by [10]:

$$\phi(\mathbf{r}_{ij}, \hat{\mathbf{r}}_{\alpha i}, \hat{\mathbf{r}}_{\beta j}) = \phi_{HS}(r_{ij}) + \sum_{\alpha,\beta} \phi_{ij,\alpha,\beta}(\mathbf{r}_{ij}, \hat{\mathbf{r}}_{\alpha i}, \hat{\mathbf{r}}_{\beta j}), \tag{2.1}$$

where $\mathbf{r}_{ij}$ is the vector of length r_{ij} connecting the centre of particle i to the centre of particle j and $\hat{\mathbf{r}}_{\alpha i}$ ($\hat{\mathbf{r}}_{\beta j}$) is the unit vector pointing from the centre of particle i (j) to the centre of patch α (β) on its surface. ϕ_{HS} is the repulsive hard sphere potential:

$$\phi_{HS}(r_{ij}) = \begin{cases} \infty, & r_{ij} < \sigma_{ij} \\ 0, & r_{ij} \geq \sigma_{ij}. \end{cases} \tag{2.2}$$

Hence, only configurations in which the particles do not overlap are possible. σ_{ij} is the distance between the centers of the particles i and j when they are in contact, see Fig.2.1(a). That is:

$$\sigma_{ij} = \frac{\sigma_i + \sigma_j}{2}, \tag{2.3}$$

where σ_i is the particle diameter of species i. For equal size mixtures σ_{ii} is just the particle diameter. $\phi_{ij,\alpha,\beta}(\mathbf{r}_{ij}, \hat{\mathbf{r}}_{\alpha i}, \hat{\mathbf{r}}_{\beta j})$ is the attractive interaction between patch α on particle i and patch β on particle j. It is generally chosen in such a way that $\phi_{ij,\alpha,\beta}(\mathbf{r}_{ij}, \hat{\mathbf{r}}_{\alpha i}, \hat{\mathbf{r}}_{\beta j}) = \phi_{ij,\alpha,\beta}(\mathbf{r}_{\alpha\beta})$, where $\mathbf{r}_{\alpha\beta} = \mathbf{r}_{ij} - \mathbf{r}_{\alpha i} + \mathbf{r}_{\beta j}$ is the vector connecting site α on particle i with site β on particle j [26], see Fig.2.1(a). A common choice for the potential [27] is the square well potential:

$$\phi_{ij,\alpha,\beta}(\mathbf{r}_{\alpha\beta}) = \begin{cases} -\varepsilon & r_{\alpha\beta} \leq d_{\alpha\beta} \\ 0 & r_{\alpha\beta} > d_{\alpha\beta} \end{cases} \tag{2.4}$$

where $\varepsilon > 0$ is the site-site energy scale, and $d_{\alpha\beta}$ are the wells widths. With these two parameters the bonding volume, i.e. the volume available to each bond can be defined [28]:

$$v_{b,ij}^{\alpha\beta} = \frac{\pi d_{\alpha\beta}^4}{30\sigma_{ij}^2}(15\sigma_{ij} + 4d_{\alpha\beta}) \tag{2.5}$$

The choice of simple discontinuous pair potentials guarantees that bonding is properly defined: a bond sets up when two patches are closer than the patch attraction range. In that case the pair interaction energy is equal to the depth of the square well. At the level of approximation we work, choosing another attractive potential would not change the results qualitatively. A possible alternative would be the potential originally introduced by Bol [29], which has subsequently become known as the Kern-Frenkel potential [30].

2.1 Wertheim's theory

The choice of a hard core repulsive interaction and that of an attractive site–site interaction of a square-well type is motivated by Wertheim's first order perturbation theory (TPT1) [31]. This mean-field theory treats the thermodynamic properties of mixtures of particles with directional interactions.

The central idea of perturbation theories is the existence of a reference system for which everything is known—structure and thermodynamics—and which is, in some sense, sufficiently close to the real system for the difference to be handled by means of an expansion in some small parameter [32]. In the case of Wertheim's theory, the unperturbed reference system is the hard-core fluid and the perturbation is the attractive bonding interaction. Considering that the attractive interaction between particles is sufficiently strong to promote association could mean that treating it as a perturbation would not work. In Wertheim's approach this difficulty is circumvented by treating different association aggregates as distinct species, each one described by a separate single particle density within a 'multi-density' formalism. The theory is based on the activity expansion of the grand partition function, which can be represented by a sum of topologically distinct diagrams. Ultimately it leads to an expression for the free energy in terms of the densities of particles in different bonding states [33].

In its simplest form, Wertheim's theory comes with the assumption that the conditions of steric incompatibilities are satisfied, i.e. bonding sites distributed on a particle's surfaces are such that two particles can form only one single bond, involving two bonding sites only, one on each particle and there is a minimum distance between sites to ensure that no sites are shaded by nearby bonds (particles do not form ringlike structures). These approximations will work better for certain systems (see Fig.2.1(b)) depending on the design, functionality and size of the particles. But they have also been relaxed for more complex situations [34]. A detailed description of Wertheim's theory can be found elsewhere [27, 31].

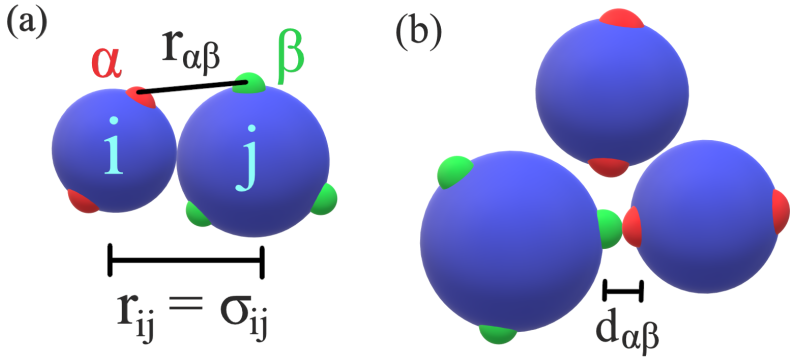

Figure 2.1: **(a)** Schematic representation of two hard-spheres at contact, the hard spheres are represented by blue circles, the small circles represent the attractive patches. The functionality of species i is $f_i = 2$ and that of species j is $f_j = 3$ **(b)** A simple interaction–site model. The range of the square-well potential $d_{\alpha\beta}$ is sufficiently short to ensure that multiple bonding at any association site is forbidden, since that would require hard spheres to overlap.

The Helmholtz free energy per particle, f_H, can then be written as a sum of two contributions: the unperturbed reference contribution, where particles only interact via their hard-core repulsion forces, f_{HS}, and the perturbation due to the attractive bonding interactions, f_b:

$$f_H = f_{HS} + f_b. \tag{2.6}$$

The unperturbed term f_{HS}, may be expressed as the sum of the ideal gas term that accounts for the kinetic energy (thermal energy) and the excess term that accounts for the excluded volume, $f_{HS} = f_{id} + f_{ex}$. For a binary mixture f_{id} is given exactly by,

$$\beta f_{id} = \ln\rho - 1 + \sum_{i=1,2} x^{(i)} \ln(x^{(i)}\lambda_i^3), \tag{2.7}$$

with $\beta = 1/k_B T$ the inverse thermal energy, $\rho = N/V$ the total number density (N is the total number of particles), $x^{(i)} = N_i/N$ the molar fraction of species i (N_i is the number of particles of species i) and λ_i^3 the thermal volume (see appendix 6.1 for details). For the excess part we use the recent equation of state proposed by Santos, Yuste, and Haro [35], which is based on the Carnahan-Starling equation of state for hard-sphere mixtures (a rather accurate equation of state for hard-sphere mixtures):

$$\beta f_{ex} = \ln(1-\eta)(-1 + C_2 - 2C_3) + \frac{\eta}{1-\eta}(3C_1 + \frac{C_2}{1-\eta} + C_3(\eta - 2)), \tag{2.8}$$

where $\eta = \frac{\pi}{6}\rho\left\langle\sigma^3\right\rangle$ is the packing fraction of the mixture, $\langle\sigma^n\rangle = \sum_i x^{(i)}\sigma_i^n$ denotes the moments of the diameter distribution. The constant terms are given by

$$C_1 = \frac{<\sigma><\sigma^2>}{<\sigma^3>}, \quad C_2 = \frac{<\sigma^2>^3}{<\sigma^3>^2}, \quad C_3 = \frac{<\sigma^2>}{<\sigma^3>^2}(<\sigma><\sigma^3> - <\sigma^2>^2). \tag{2.9}$$

See appendix 6.2 for details on how to go from the equation of state to the excess free energy, Eq.(2.8). The bonding free energy is approximated by Wertheim's theory and comprises two contributions, the bonding energy and an entropic term related to the number of ways of bonding two particles. It is given by,

$$\beta f_b = \sum_{i=1,2} x^{(i)} \left[\sum_{\alpha\in\Gamma(i)} \left(\ln X_\alpha^{(i)} - \frac{X_\alpha^{(i)}}{2} \right) + \frac{1}{2} f^{(i)} \right], \tag{2.10}$$

where $\Gamma(i)$ is the set of bonding sites on one particle of species $i = \{1,2\}$ and $f^{(i)} = \sum_{\alpha\in\Gamma(i)} f_\alpha^{(i)}$ is the total number of bonding sites per particle of species i (the functionality). $X_\alpha^{(i)}$ is the probability that a site of type α on a particle of species i is not bonded. This probability is related to the total density, molar fractions and temperature through the laws of mass action. These are obtained by treating bond formation as a chemical reaction:

$$X_\alpha^{(i)} = \left[1 + \rho \sum_{j=1,2} x^{(j)} \sum_{\gamma\in\Gamma(j)} X_\gamma^{(j)} \Delta_{\alpha\gamma}^{(ij)} \right]^{-1}, \tag{2.11}$$

$\Delta_{\alpha\gamma}^{(ij)}$ characterises the bond between a site α on a particle of species i and a site γ on a particle of species j: it is the probability of forming a bond, once the available sites of the two particles are chosen. It depends on how the patches are modeled. For spherical patches interacting via square wells with depths

$\varepsilon_{\alpha\beta}$ and considering that only inter-species bonding is allowed means that in order for a bond to form, two particles of different species have to come in contact. Therefore, the well depths are simply $\varepsilon_{\alpha\beta} = \varepsilon$, i.e. there is a single energy scale. The probability is different than zero only for $\Delta^{(ij)}_{\alpha\gamma} = \Delta^{12}_{AB} = \Delta$ and it is given by

$$\Delta = \int_{v_b} g^{(12)}_{HS}(\mathbf{r})[\exp(\beta\varepsilon) - 1]d\mathbf{r}, \tag{2.12}$$

where $g^{(12)}_{HS}(\mathbf{r})$ is the radial distribution function of the reference hard sphere fluid for two particles of different species and the integral is calculated over the bonding volume, v_b, which is constant since there is a single type of bond (between different species). $g^{(12)}_{HS}(\mathbf{r})$ is approximated by its contact value $A_o(\eta)$, as obtained from Santos [35] (also based in the Carnahan–Starling contact value):

$$A_o(\eta) = \frac{1}{1-\eta} + \frac{3}{2}\frac{\eta(1-\eta/3)}{(1-\eta,)^2}Z + \frac{\eta^2(1-\eta/2)}{(1-\eta)^3}Z^2, \tag{2.13}$$

where $Z = 2\frac{<\sigma^2>}{<\sigma^3>}(\frac{1}{\sigma_1} + \frac{1}{\sigma_2})^{-1}$ (Z^{-1} represents an average curvature). Using $g^{(12)}_{HS}(\mathbf{r}) = A_o(\eta)$, Eq. (2.12) becomes

$$\Delta = v_b[\exp(\beta\varepsilon) - 1]A_o(\eta). \tag{2.14}$$

These approximations are in line with the independent site approximation underlying Wertheim's theory and will affect the results quantitatively, but are not expected to change them qualitatively.

2.2 Phase separation: Stability

For binary mixtures, besides mechanical instability (due to density fluctuations), strong composition fluctuations can lead to material instability. The latter lead to demixing, i.e. a separation of the system into phases of different compositions. The phase separation of a solution often results in the coexistence of a high density phase (liquid phase) and a low density phase (vapor phase).

The equilibrium properties of the mixture can be determined by minimising (at a fixed composition x, pressure p and temperature T) the Gibbs free energy per particle:

$$g = \frac{p}{\rho} + f_H, \tag{2.15}$$

with respect to the total density ρ, subject to the constraints imposed by the law of mass action Eq. (2.11). A standard Newton–Raphson method is used to minimise $g(x)$, and the law of mass action is solved analytically. Binodal lines (the lines that indicate where phase separation occurs) are located by a standard common-tangent construction on $g(x)$, which is equivalent to solving the equations for the equality of the chemical potentials of both species in the coexisting phases [36]. Mechanical and thermal equilibria are satisfied by fixing both the pressure and the temperature. Critical points (the points at which both phases of a substance have the same density, and are therefore indistinguishable) are computed by determining the states which satisfy the law of mass action, Eq. (2.11), and the spinodal condition:

$$f_{vv}f_{xx} - (f_{xv})^2 = 0, \tag{2.16}$$

where subscripts denote partial derivatives, i.e. f_{xv} is the second partial derivative of f_H with respect to the reduced volume per particle $v = 1/\eta$ and the composition x at constant temperature. In addition,

stability requires the vanishing of the third-order derivative in the direction of maximal growth [37]:

$$f_{xxx} - 3f_{xxv}\left(\frac{f_{xv}}{f_{vv}}\right) + 3f_{xvv}\left(\frac{f_{xv}}{f_{vv}}\right)^2 - f_{vvv}\left(\frac{f_{xv}}{f_{vv}}\right)^3 = 0 \tag{2.17}$$

In what follows, we denote the composition of the mixture x by the molar fraction of species 1: $x^{(1)} = x$. Hence, the molar fraction of species 2 is $x^{(2)} = 1 - x$.

2.3 Aggregation: Percolation

A system of patchy particles may form a gel if the probability of finding an infinite spanning cluster is nonzero. When a system begins to percolate, it transforms from a viscous liquid into an elastic disordered solid [38], which in addition to the direct change of the viscoelastic properties, may lead to changes in the physical response properties, e.g. its electric conductivity.

In order to study percolation we use the generalization of the Flory-Stockmayer [39, 40] random-bond percolation model by Tavares et al. [41]. Consistent with the assumptions made in Wertheim's theory, closed loops are neglected and the clusters assume a tree-like bonding structure as shown in Fig. 2.2. Hence, the connections of a cluster are separated by levels: a random particle is chosen as the level 0; the particles directly connected to this are at level 1, and so-forth. Let $n^{(k)}_{i+1,\gamma}$ denote the number of bonded sites γ on particles of species k at the level $i+1$. This number is related to the number of all types of bonded sites of both species of particles in the previous level $n^{(j)}_{i,\alpha}$ through the recursion relation:

$$n^{(k)}_{i+1,\gamma} = \sum_j \sum_{\alpha\in\Gamma_d(j)} \sum_{\beta\in\Gamma_d(j)} p_{\beta_j\to\gamma_k}(f^{(j)}_\beta - \delta_{\beta\alpha}) n^{(j)}_{i,\alpha}. \tag{2.18}$$

The sum on j runs over the particle species, $j = \{1,2\}$, $\Gamma_d(j)$ is the set of different bonding sites on species j, $p_{\beta_j\to\gamma_k}$ is the probability of bonding a site β on a particle of species j to a site γ on a particle of species k and $\delta_{\beta\alpha}$ is the Kronecker delta. By summing this probability over the particles species and the different sites, the probability of finding a bonded site β on a particle of species j is found:

$$P_{\beta_j} = \sum_k \sum_{\gamma\in\Gamma_d(k)} p_{\beta_j\to\gamma_k}, \tag{2.19}$$

This can be traced back to the laws of mass action (Eq. 2.11), and therefore to the thermodynamic variables considering that:

$$P_{\beta_j} = 1 - X^{(j)}_\beta. \tag{2.20}$$

In order to find if the system has percolated, we express Eq. (2.18) in matrix form :

$$\tilde{n_i} = \tilde{T}^i \tilde{n_0}, \tag{2.21}$$

where $\tilde{n_i}$ is a vector with components $n^{(k)}_{i,\gamma}$ and $\tilde{T}$ is a square matrix (the transition matrix) that encodes the connectivity properties of the cluster. The elements of $\tilde{T}$ are given by:

$$T_{\gamma_k\alpha_j} = \sum_{\beta\varepsilon\Gamma_d(j)} p_{\beta_j\to\gamma_k}(f^{(j)}_\beta - \delta_{\beta\alpha}). \tag{2.22}$$

$\tilde{T}$ has dimensions equal to the number of particle species multiplied by the number of distinct bonding sites and may be diagonalized or transformed into Jordan form. In either case, the progressions defined

by Eq. (2.18) converge to zero if the largest (absolute value) of the eigenvalues λ_{γ_k} of $\tilde{T}$ is less than unity, i.e. $|\lambda_{\gamma_k}| < 1$ because this means the number of bonds decreases with increasing level. The percolation threshold is then reduced to determining the thermodynamic states for which the largest absolute value of the eigenvalue, $|\lambda_{\gamma_k}|$, of matrix $\tilde{T}$ is equal to unity. This means the system will be percolated if the number of bonds increases with increasing level. For more details see Refs. [18, 41].

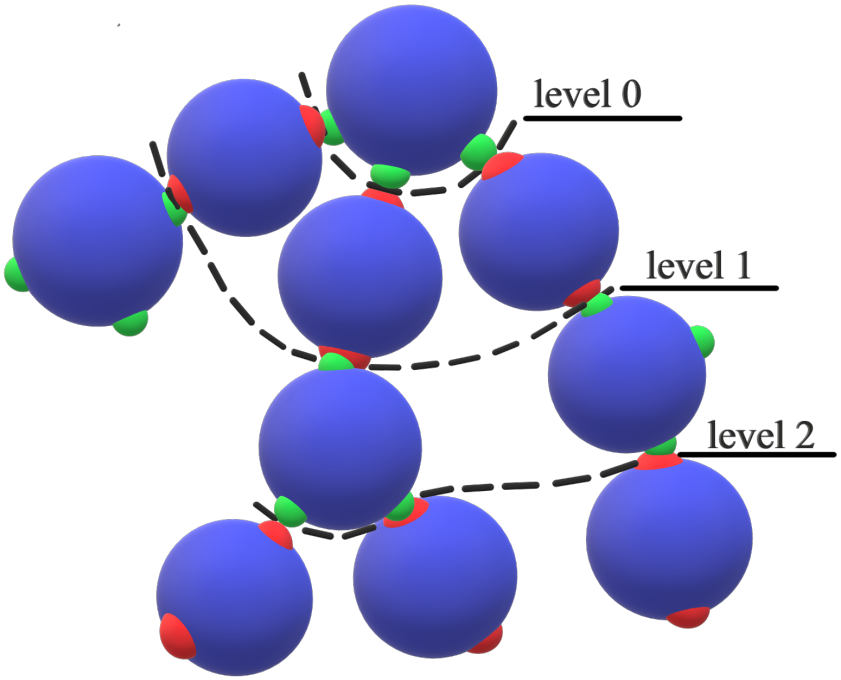

Figure 2.2: Schematic representation of a treelike cluster in a binary mixture. After choosing a random particle (top of figure), the cluster can be represented by levels as shown. On each level there are n_i bonded sites. A bond between two bonding sites lowers the energy by ε.

The average size of the clusters, $\langle M \rangle$, will give us some insight on the structure of the fluid, by definition:

$$\langle M \rangle = \frac{N}{N_{cl}}, \tag{2.23}$$

where N is the total number of particles and N_{cl} is the number of clusters. Under the no-loop assumption, the number of clusters is $N_{cl} = N - N_{bonds}$, where N_{bonds} is the number of bonds. Hence, for every bond the number of clusters is reduced by one. One can rewrite Eq.(2.23) as $\langle M \rangle = (1 - N_{bonds}/N)^{-1}$. In this way, the number of bonds per particle is calculated considering the bonding probabilities:

$$\frac{N_{bonds}}{N} = \frac{f^{(1)}x(1-X_A) + f^{(2)}(1-x)(1-X_B)}{2}, \tag{2.24}$$

where $f^{(i)}$ are the functionalities of each particle species. Plugging Eq.(2.24) into Eq.(2.23) gives the expression for the average size of the clusters.

Chapter 3

Bulk Phase Behavior

We study the particular case of a binary mixture with a different number of distinct bonding sites (Fig. 3.1). We consider that particles of species 1 have $f^{(1)}$ patches of type A and diameter σ_A - these are the linker species - and particles of species 2 have $f^{(2)}$ patches of type B and diameter σ_B - they are the monomer species. The fact that only inter-species bonding is allowed defines a single energy scale. Therefore, species i can be referenced with respect to its type of patch. The particular case considered here has $f^{(1)} = f_A = 2$ and $f^{(2)} = f_B = 3$. In what follows species 1 is denoted as species A (or $2A$) and species 2 as species B (or $3B$).

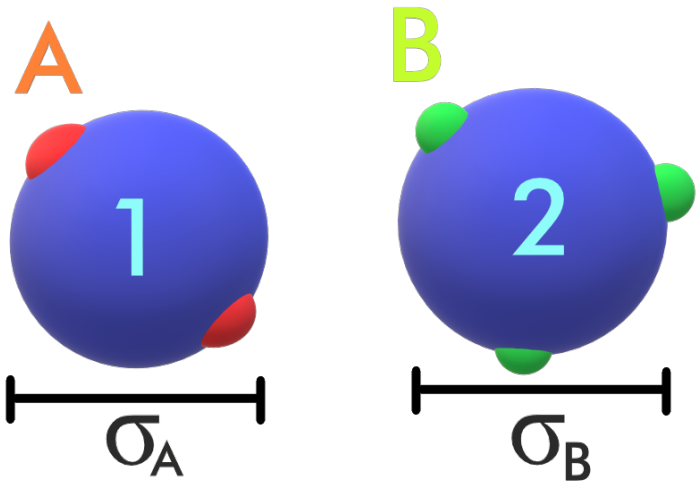

Figure 3.1: Particle model. Particles of species 1 have diameter σ_A and 2 patches of type A . Particles of species 2 have diameter σ_B and 3 patches of type B. This mixture is referred to as a 2A-3B mixture.

3.1 Phase diagram for the 2A-3B mixture

We start by writing the bonding energy for this system. From equation (2.10) with $\Gamma(1) = A$, $\Gamma(2) = B$, $X_\alpha^{(1)} = X_A$, $X_\alpha^{(2)} = X_B$ we get:

$$\beta f_b = x f_A \left[\ln(X_A) - \frac{X_A}{2} + \frac{1}{2} \right] + (1-x) f_B \left[\ln(X_B) - \frac{X_B}{2} + \frac{1}{2} \right]. \tag{3.1}$$

The laws of mass action form a system of two coupled equations for the fraction of unbounded sites

A and B, from Eq. (2.11)

$$\begin{aligned} 1-X_A &= \rho f_B(1-x)X_B X_A \Delta, \\ 1-X_B &= \rho f_A x X_A X_B \Delta. \end{aligned} \tag{3.2}$$

Which is solved analytically. The percolation matrix is determined from Eq. (2.22) and Eq. (2.19) with $P_{A_2} = P_{B_1} = 0$, $P_{A_1} = p_{A_1 \to B_2}$ and $P_{B_2} = p_{B_2 \to A_1}$. The matrix is:

$$\begin{pmatrix} 0 & P_{B_2}(f_B - 1) \\ P_{A_1}(f_A - 1) & 0 \end{pmatrix}, \tag{3.3}$$

which can be related to the thermodynamic variables through the laws of mass action since $P_{A_1} = 1 - X_A$ and $P_{B_2} = 1 - X_B$:

$$\begin{pmatrix} 0 & (1-X_B)(f_B - 1) \\ (1-X_A)(f_A - 1) & 0 \end{pmatrix}. \tag{3.4}$$

And the eigenvalues of this matrix are:

$$\lambda_{\pm} = \pm\sqrt{(1-X_B)(f_B-1)(1-X_A)(f_A-1)}. \tag{3.5}$$

The percolation threshold is reached when the eigenvalue λ_+ is equal to unity.

The bulk phase diagram for the equal size mixture, $\sigma_A = \sigma_B$, in the composition-temperature plane for the fixed pressure $P^* = pv_A/\varepsilon = 7 \cdot 10^{-5}$ is shown in Fig. 3.2.

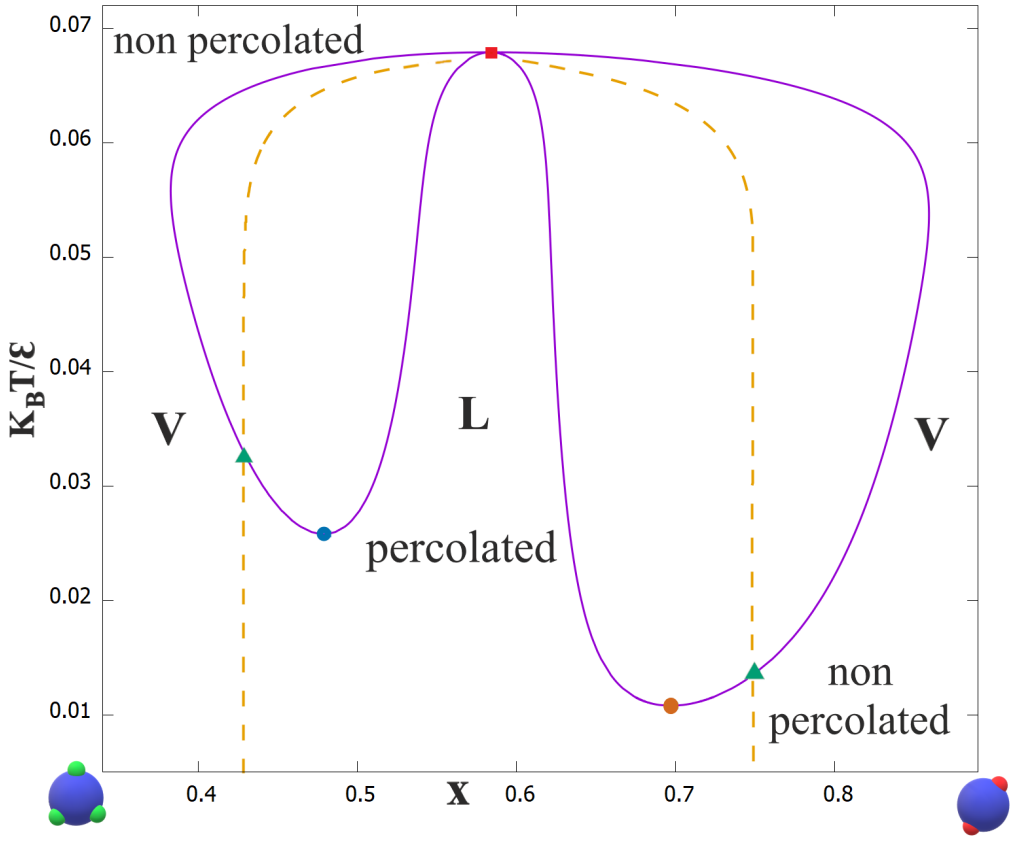

Figure 3.2: Bulk phase diagram of the equal size mixture in the composition-temperature plane for the reduced pressure $P^* = pv_s/\varepsilon = 7 \cdot 10^{-5}$. The solid violet line is the binodal, which defines the coexistence region, the brown circle is the critical point of the phase rich in 2A and the blue circle the critical point of the phase rich in 3B. The red square is the azeotropic point. The dashed orange lines are the percolation lines that enter the coexistence regions through the green triangles. **V** represents the vapor phase and **L** the liquid phase.

There are two coexistence regions: one dividing a region where we have a vapor-phase (low and high composition) and a liquid-phase (middle region). The number of bonds is controlled by the composition of both species. The monomer species $3B$ allows for 3 bonds per particle, but since we are only considering inter-species bonds, this means we need more 2A particles overall to potentially have a fully connected system. The ground state, where all patches are bonded, happens when the compositions of the $2A$ and $3B$ are $x = 0.6$ and $(1-x) = 0.4$, respectively. This is why we have the denser phase for values around $x = 0.6$ for which most bonds are realizable. The vapor phases that exist at low temperatures occur when the mixture is mostly made of one of the species. At high temperatures the system is in a vapor phase for all compositions, this is because the kinetic energy of the particles overcomes the potential bonding energy and no bonds are present. The asymmetry in the coexistence regions (the 2A rich coexistence region extends to lower temperatures and a wider range of compositions than the 3B) is due to the different functionality of the particles.

It is not possible to classify this mixture following van Konynenburg and Scott [42], as none of the two pure fluids undergoes liquid-vapor (LV) condensation, i.e. the coexistence regions do not extend to the pure fluid compositions, $x = 0$, $x = 1$. A negative azeotropic point is present at $x \approx 0.58$: this is a constant boiling point where the liquid and vapor phases have the same composition and the transition is of first order. Two lower critical points are shown. For these points the liquid and vapor phases are indistinguishable. The percolation lines were also obtained. They indicate the percolation threshold, meaning that in between the lines the system percolates. The liquid phase is always percolated (which means the liquid phase is always a network fluid). Inside the coexistence regions and close to the critical points the system divides into a percolated vapor phase and a percolated liquid phase . Moving away from the critical points, the system divides into a percolated liquid and non percolated vapor. The percolation lines enter the coexistence region in the percolation end points (green triangular points), these points will be important when the effect of gravity is considered. As the temperature is increased the percolation lines approach similar values and finally meet in the azeotropic point. When $T \to 0$ the percolation lines tend to $x \approx 0.43$ (with $X_A \to 0$ and $X_B \to 0.5$) in the phase rich in $3B$ and to $x = 0.75$ (with $X_A \to 0.5$ and $X_B \to 0$) in the phase rich in $2A$.

In Fig. 3.3 the pressure dependence is investigated. We show the bulk phase diagrams in the composition-temperature plane for different values of the pressure. The two phase regions shrink when pressure is increased, meaning that pressure forces the system to mix. Increasing the pressure leads to a density increase (see Eq. (2.15)), which explains why the system is more prone to mix (if only homogeneous phases are considered). For pressures higher than $P^* = 1.94 \cdot 10^{-4}$ the 3B rich coexistence region disappears and we are left with a closed miscibility gap with upper and lower critical points inside a percolated region. This gap also divides the system in a liquid (denser) phase for compositions closer to $x \approx 0.6$ and a vapor phase (less dense) for compositions farther away from $x \approx 0.6$. For pressures above $P^* = 3.9 \cdot 10^{-4}$ the LV condensation disappears and the system is completely miscible. The percolation lines show a similar behavior. Percolation lines are not plotted inside the coexistence region. The closed miscibility gap is completely inside the percolated region.

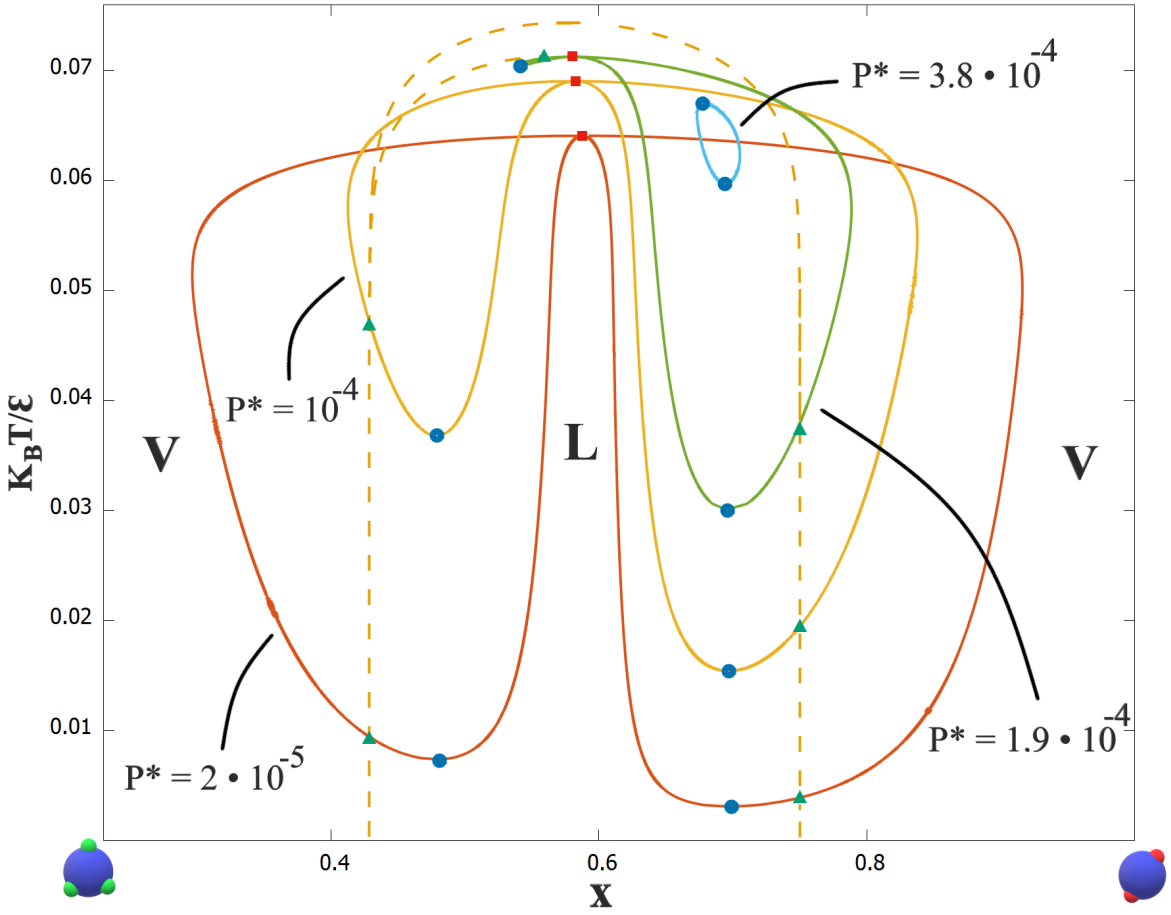

Figure 3.3: Bulk phase diagrams in the composition-temperature plane for the reduced pressure $P^* = 2 \cdot 10^{-5}$ (orange line), $P^* = 10^{-4}$ (yellow line), $P^* = 1.9 \cdot 10^{-4}$ (green line) and $P^* = 3.8 \cdot 10^{-4}$ (blue line). The topology of the phase diagram changes for this last value. Blue circles are the critical points and red squares the azeotropic points. The percolation lines are represented in dashed yellow lines, they end in the green triangles (at coexistence region).

In Fig. 3.4 we represent the critical properties of the mixture. In Fig. 3.4 (a) the critical lines in critical temperature versus critical packing fraction representation are shown. There is no empty liquid regime since the critical lines do not tend to zero (if this were the case it would be possible to have fluid phases at arbitrarily low densities). Nevertheless, the critical lines tend asymptotically to $\eta_C^- \approx 0.0189$ in the phase rich in 3B and to $\eta_C^+ \approx 0.0246$ in the phase rich in 2A, which are relatively low values for fluid phases. In Fig. 3.4(b) critical pressure-critical temperature projections are represented. The critical line forms a closed loop starting and ending at $p \to 0$ and $T \to 0$. In Fig. 3.4 (c) we show the critical bonding probabilities, $(1 - X_A)$ and $(1 - X_B)$ dependence on the critical temperature. In the 2A rich phase, all 3B patches are bonded ($(1 - X_B) \to 1$), and the opposite happens for the 3B rich ($(1 - X_A) \to 1$). The probability of finding a bonded 2A patch in the 2A rich phase tends to $(1 - X_A) \to 0.67 \approx 2/3$ which is the proportion of different types of bonds, 2A-3B. This is a consequence of considering interspecies bonding. It is as if for each $2A$ particle there's a $3B$ particle. In the 3B rich phase the probability of finding a bonded 3B patch tends to $(1 - X_B) \to 0.61$. In Fig.3.4 (d) the critical average size of the clusters $\langle M \rangle$ is studied, the average size of the clusters as $T \to 0$ in the 2A rich phase tends to $\langle M \rangle^+ \to 10.9$ and in the 3B rich to $\langle M \rangle^- \to 23.7$. The phase richer in 3B has a bigger average cluster size because these particles allow for more bonds. As the critical temperature increases, they approach similar values.

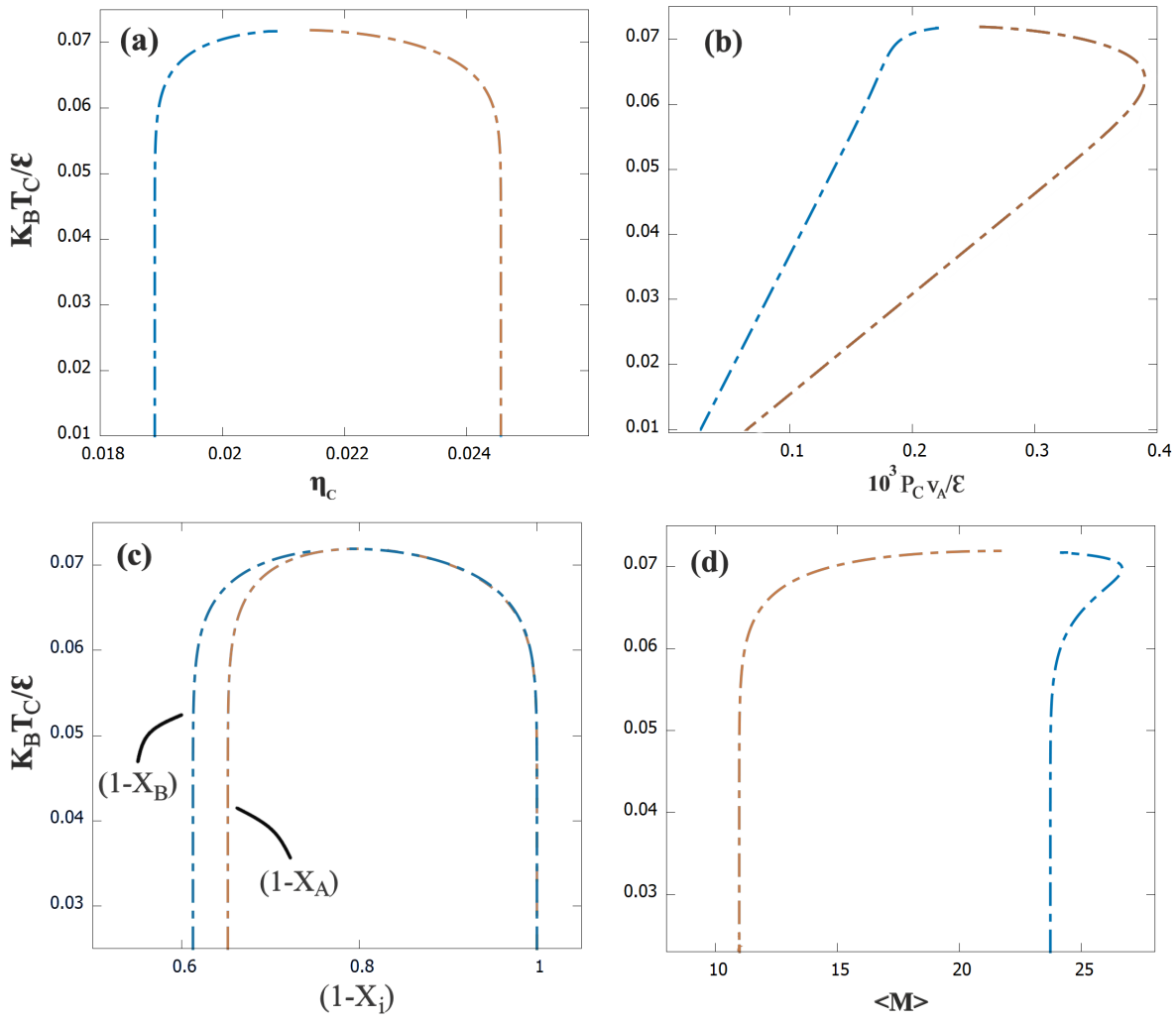

Figure 3.4: Critical properties of the equal size mixture, the critical lines corresponding to the phase richer in 2A are in brown and in blue for the phase richer in 3B. (a) critical temperature versus critical packing fraction, (b) critical temperature-critical pressure. (c) critical bounding probabilities-critical temperatures. (d) critical temperature-critical average size of the clusters.

3.2 The effect of size: Different size mixtures

Next we study the effect of changing the relative size of the particles $\sigma^* = \sigma_B/\sigma_A$ on the phase behavior of the mixture. We consider the range $\sigma^* = [1, 1.95]$ and in Fig. 3.5 we plot the phase diagrams for different size mixtures at a fixed pressure $P^* = 7 \cdot 10^{-4}$.

The phase diagrams have the same topologies as before: as σ^* increases the coexistence regions gets smaller, similar to the effect of increasing the pressure in the case of equal sized mixtures. Above $\sigma^* = 1.63$ the 3B rich phase disappears and the topology of the phase diagrams changes to a closed miscibility gap; above $\sigma^* = 1.95$ the gap disappears and the system becomes completely miscible at all temperatures.

Increasing the relative size of the particles can be achieved by increasing the size of the 3B particles or decreasing the size of the 2A particles; the size of the patches does not change since the bonding volume remains constant throughout. By increasing the size of the 3B particles we increase the interspecies excluded volume and particles have less volume to explore, making it harder to bond causing the miscibility gaps to shrink. Equivalently, by making 2A particles smaller the interspecies excluded

volume is reduced, resulting in the mixing of the components, due to the increase in the multiplicity of ways of mixing them. In what follows, the change in σ^* was performed by increasing the size of the 3B particles. The size of the 2A particles remained constant throughout. The calculation of the binodal in the critical region is incomplete. This is due to a numerical problem caused by the difficulty of minimizing the functional g near the critical region. Ways of solving this problem have been and still are being implemented. Nevertheless, we do not expect this region to change considerably since the calculation of the critical properties, in the composition-temperature plane (not shown) showed that the critical point would appear in the incomplete region. In a similar way, the percolation lines show that the liquid phase is always percolated. The behavior of the percolation lines changes only slightly by changing the size. This is because the size dependence in the eigenvalues Eq.(3.5) is in the probabilities $(1-X_i)$ and as it is shown below, the effect of changing the size makes $(1-X_A)$ increase and $(1-X_B)$ decrease, which compensate one another, causing the value of λ_{12} to change very little. The asymptotic behavior of the percolation lines does not change by changing σ^* (in a similar fashion to what happened by increasing the pressure). The phase rich in 3B tends to $x \approx 0.43$ (with $X_A \to 0$ and $X_B \to 0.5$) and the phase rich in 2A to $x = 0.75$ (with $X_A \to 0.5$ and $X_B \to 0$). Inside the coexistence regions the lines continue and meet in the azeotropic point. For the closed miscibility gap, by contrast to what happened before, the gap is not completely inside the percolated region, and it crosses the coexistence region.

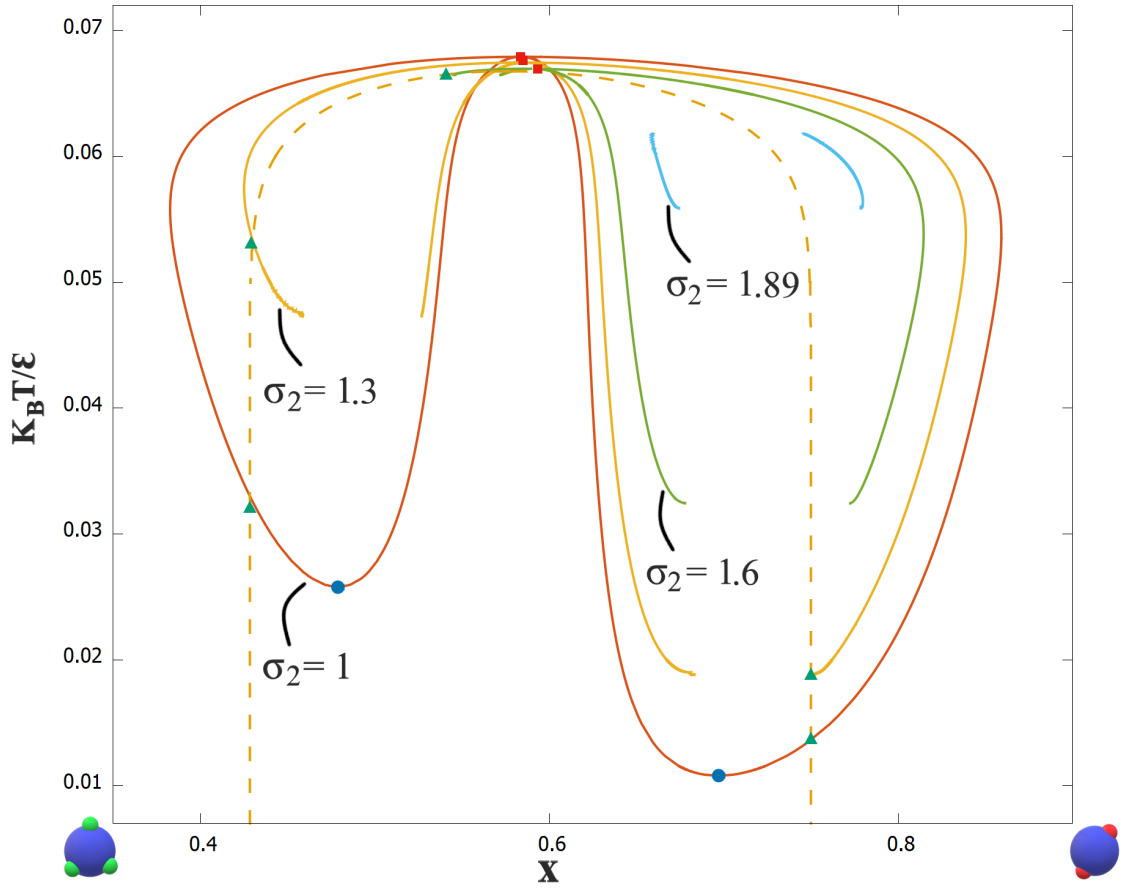

Figure 3.5: Phase diagrams in the temperature-composition plane for $P^* = 7 \cdot 10^{-5}$ and different sized mixtures. The values of σ_B/σ_A are $\sigma_B/\sigma_A = 1$ (orange line), $\sigma_B/\sigma_A = 1.3$ (yellow line), $\sigma_B/\sigma_A = 1.6$ (green line), $\sigma_B = 1.89$ (blue line). The percolation lines are plotted in dashed lines that end in the green triangular points. The open binodals are due to the difficulty of minimizing the functional near the critical region.

The critical properties of these mixtures are shown in Fig. 3.6 and the asymptotic behavior summarized in table 3.1. We refer to the critical lines of the phase richer in 3B with the superscript $-$ and the phase richer in 2A with the superscript $+$.

As we increase the size of the 3B particles the critical packing fractions of the mixture tends to higher values Fig. 3.6 (a) , this is not surprising since the system is more packed. For the PT projections in Fig.3.6 (b), the closed loops get smaller with increasing size, which is an indication that the coexistence regions get smaller. There is also a shift of the closed loops to lower critical temperatures and pressures as the size increases.

In Fig. 3.6 (c) the critical bonding probabilities are represented $(1-X_A)$, $(1-X_B)$. As the relative size of the particles is increased, in the rich in 3B phase it becomes harder to find a bonded 3B patch (2A patches are completely bonded) and in the rich in 2A phase it becomes easier to find a bonded 2A patch (3B patches are completely bonded). This describes the effect of changing the size of the particles.

The behavior of the average cluster size is the most interesting. In Fig. 3.6 (d), we see that the clusters in the 3B rich phase tend to smaller values as we are increasing σ^* (the probability of bonding a 3B particles is decreasing). In the 2A rich phase, the average size of the clusters increases (the probability of bonding a 2A particle is increasing).

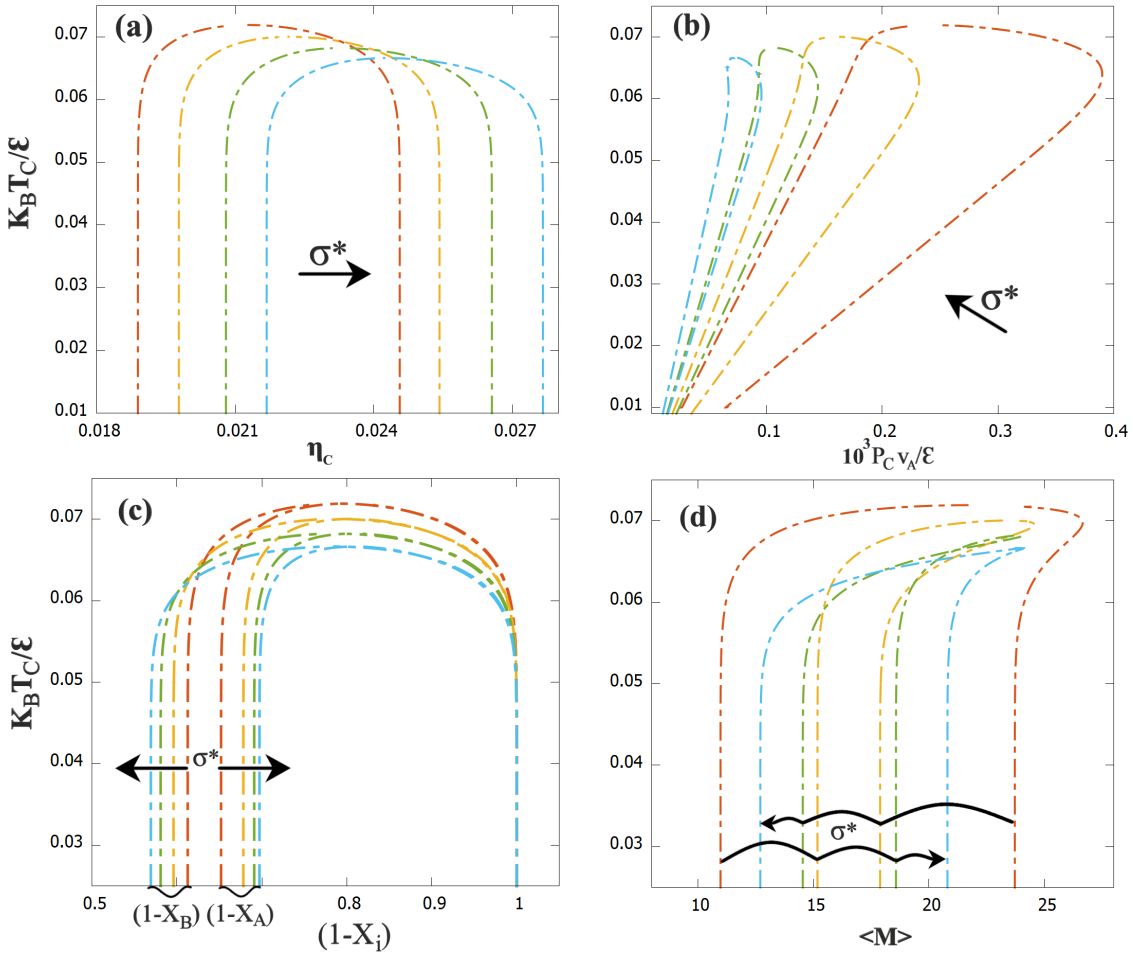

Figure 3.6: Critical properties for mixtures of different sized particles. The color scheme is the following: $\sigma_B/\sigma_A = 1$ (orange line), $\sigma_B/\sigma_A = 1.3$ (yellow line), $\sigma_B/\sigma_A = 1.6$ (green line), $\sigma_B/\sigma_A = 1.89$ (blue line). The arrows represents the direction of increasing σ_B/σ_A. (a) critical temperature versus critical packing fraction, (b) critical temperature-critical pressure. (c) critical bonding probabilities-critical temperatures. (d) critical temperature-critical average size of the clusters.

	η_C^-	η_C^+	$\langle M\rangle^-$	$\langle M\rangle^+$	$(1-X_A)^-$	$(1-X_B)^+$
$\sigma^* = 1$	0.0189	0.0246	23.7	10.9	0.67	0.61
$\sigma^* = 1.3$	0.0198	0.0254	17.9	15.2	0.68	0.6
$\sigma^* = 1.6$	0.0208	0.0265	14.5	18.6	0.69	0.58
$\sigma^* = 1.89$	0.0217	0.0276	12.7	20.8	0.7	0.57

Table 3.1: Critical values of the system as the temperature vanishes, $T \to 0$. The phase rich in 3B is denoted by the index $-$ and the rich phase rich in 2A is denoted by the index $+$

3.3 Other representations of the phase diagram

In a colloidal experiment, as the presence of gravitational effects is often unavoidable, it is more informative to represent the phase diagrams with the conditions that are possible to achieve in a lab. To do so, we need for example pressure-composition diagrams at constant temperature, as these are easier variables to control in a lab. Furthermore, the theory developed in chapter **4** to calculate the stacking diagram requires the chemical potential representation of the phase diagram, μ_2 vs μ_1. With this in mind, in Fig. 3.7 two pressure-composition diagrams and their corresponding chemical potential diagrams are calculated. The pressure-composition diagrams are obtained in a similar fashion as the previous diagrams, but this time fixing the temperature. The chemical potential diagrams are obtained from the pressure-composition diagrams considering that $g = x\mu_1 + (1-x)\mu_2$. Hence, μ_1 and μ_2 are obtained from the value of the common tangent to $g(x)$ at $x = 1$ and $x = 0$ respectively.

The pressure-composition diagrams shown are representative of the system under study as they show the two possible topologies already discussed. In (Fig.3.7 (a)) a percolated closed miscibility gap with upper and lower critical points is present. For temperatures lower than $T^* = 0.071$ another coexistence region appears, the one rich in 3B particles Fig.3.7 (b), and for this we have a positive azeotropic point and two upper critical points. We also represent the percolation lines, that again, indicate the percolation of the vapor phase. At higher temperatures the region of concentrations where phase separation takes place shrinks and eventually disappears, similarly to increasing the pressure in the case of temperature-composition diagrams (Fig. 3.3). This is because the kinetic energy becomes much larger than potential energy at high T, the thermal fluctuations overcome the bonding energy and thus the system mixes.

The topological correspondence between the pressure-composition and chemical potential representation is robust (i.e. number of binodals, ending points, asymptotic behaviour of the binodals...), but certain details, such as the precise curvature of the binodals, depend on the system under consideration. The binodals in the chemical potential plane are proportional to the size of the coexistence region in the pressure-composition plane. The closed loop of immiscibility in (Fig.3.7 (a)) corresponds to a binodal that ends at two critical points in the plane of chemical potentials. The two coexistence regions in (Fig.3.7 (a)) correspond to two binodals joined by the azeotropic point and each ending at a critical point in the chemical potential representation.

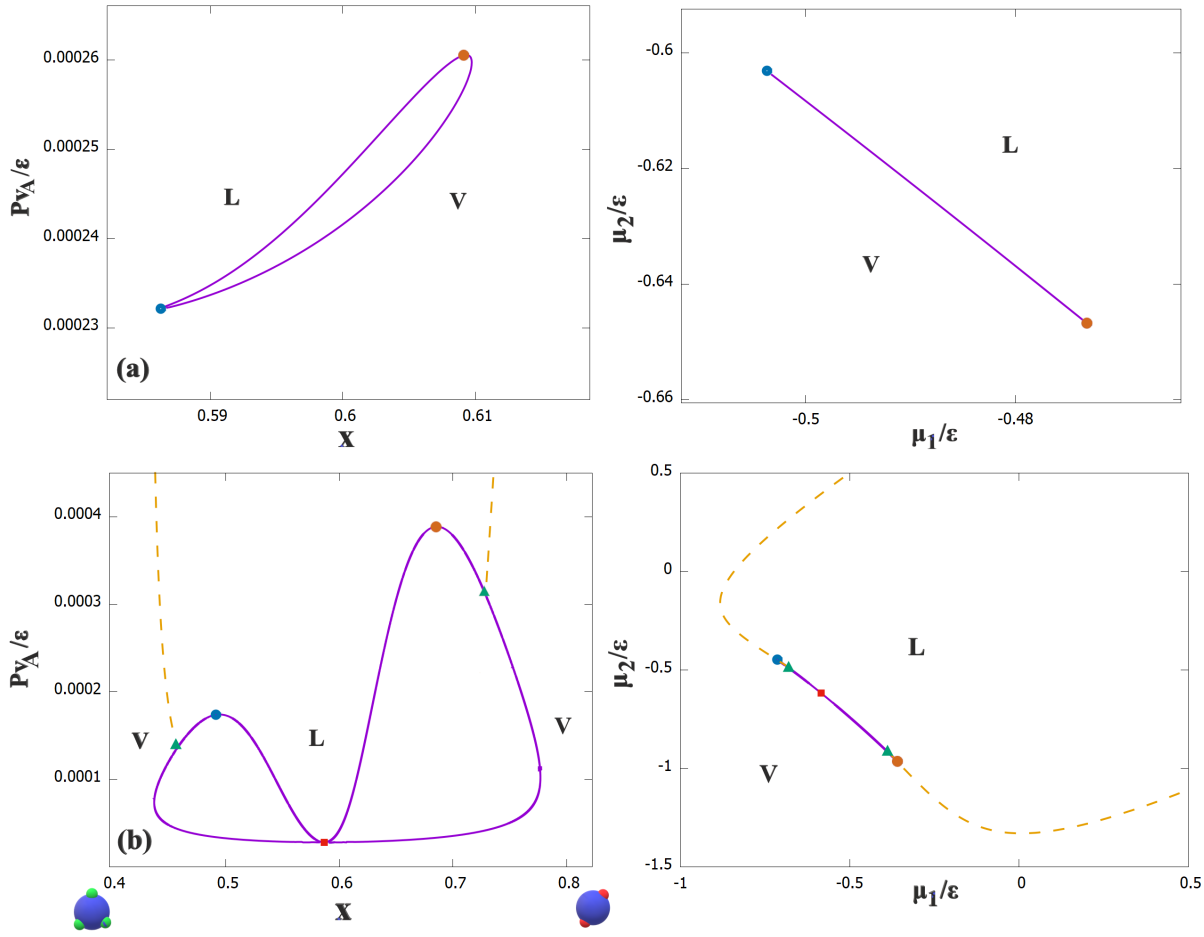

Figure 3.7: Pressure-composition diagrams at constant temperature (left panels) and corresponding chemical potential diagrams (right panels). (a) T*=0.0718, (b) T*=0.065. Violet lines indicate the binodals, yellow dashed lines are the percolation lines (not shown in (a) because the system is always percolated) that end in green triangular points. Blue dots are the critical points of the phase rich in 3B and brown points the critical points of the phase rich in 2A. The azeotropic point is represented by the red square.

Chapter 4

Sedimentation

4.1 Sedimentation: theoretical framework

Sedimentation is the progressive deposition of particles in a fluid subject to an external field, in this case, the gravitational field. Gravity can have a strong effect on colloidal systems because on typical length scales in the laboratory the gravitational energy and the thermal energy are comparable [12]. This is one of the reasons why gravitational effects are commonly used as a tool to study the collective behaviour of colloidal mixtures, see Fig. 4.1. The presence of gravity may also result in additional gravity-induced phenomenology not present in bulk systems [21]. Sedimentation experiments allow access to fundamental properties of colloids. Examples are the experiments by Perrin, which included the measurement of the Boltzmann constant [43], as well as the test of the bulk equation of state of hard spheres by Piazza et. al. [44].

The stacks that form in an experiment when sedimentation-diffusion-equilibrium is established are distinguished by the different phases the system is in. When colloidal mixtures are considered, this behavior can be quite complex, including the formation of multiple stacks as well as counterintuitive such as denser particles floating on top of lighter ones. A stacking sequence is the sequence of stacks of different phases that appear under gravity in a given sample [25].

In Fig. 4.1 the time evolution of a sedimentation experiment [22] of a colloidal mixtures of gibbsite platelets and silica spheres is shown. The vessels display different stacking sequences of isotropic and nematic phases depending on the size of the particles used. This is just an example of the behavior which is possible to obtain with colloidal mixtures.

De las Heras and Schmidt [20] developed a theory relating the bulk phase diagram to its phase stacking phenomenology under gravity via a local density approximation (LDA). As discussed below the full set of possible phase stacking sequences in sedimentation-diffusion equilibrium originates from straight lines (sedimentation paths) in the chemical potential representation of the bulk phase diagram.

The height-dependent local chemical potential for each species is defined as

$$\psi_i(z) = \mu_i^b - m_i g z, \tag{4.1}$$

where μ_i^b is the bulk chemical potential of species i, m_i is the buoyant mass of species i and g is the acceleration due to gravity. By eliminating the spatial dependency of the local chemical potentials the sedimentation path that describes the variation of local chemical potentials along the sedimented colloidal mixture is defined:

$$\psi_2(\psi_1) = a + s\psi_1. \tag{4.2}$$

Where $a = \mu_2^b - s\mu_1^b$ and $s = m_2/m_1$. This describes a straight line in the plane of local chemical potentials. If all correlation lengths in the system are small compared to the gravitational lengths $\gamma_i = k_B T/m_i g$ one can apply a local density approximation by which it is assumed that the state of the system at height z is the same as the equilibrium state of a bulk system with chemical potentials μ_i, that equal the height-dependent local chemical potentials $\psi_i(z)$. This approximation is justified considering that in colloidal systems γ is typically of the order of millimeters or centimeters. Hence, the LDA is often an accurate approximation for the system under consideration.

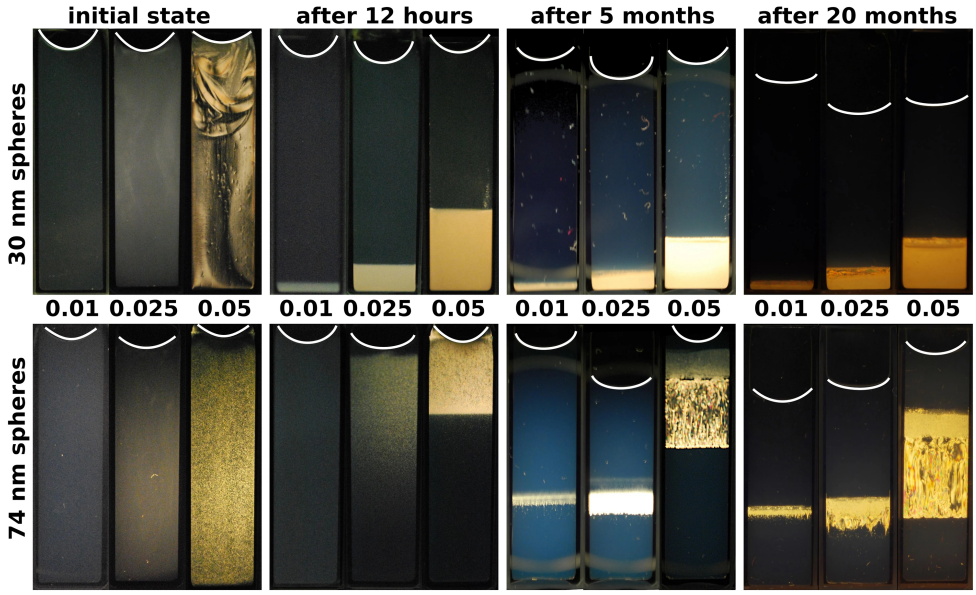

Figure 4.1: Photographs taken between crossed polarizers showing the time evolution of samples in a sedimentation experiment with colloidal mixtures of gibbsite platelets (diameter of 186 nm) and silica spheres with diameters of 30 nm (top row) and 74 nm (bottom row). The initial bare packing fraction of the spheres is 0.05, and for the platelets 0.01, 0.025, and 0.05, as indicated. The mixtures with small spheres separated into a bottom nematic (orange) and a top isotropic (black) phase. The stacking sequence of the mixtures with the larger spheres is different. The sample developed a floating nematic layer between isotropic bottom and top layers. Taken with permission from Ref.[22]

We will consider the limit of samples with very large (infinite) height: in this case, the sedimentation path is fully defined by its slope s, intercept a and direction, given by the sign of the buoyant masses (if m_i is positive the $\mu_i(z)$ decreases from bottom to top of the sample). This limit is justified considering that in a standard sedimentation experiment of colloidal mixtures the length of the sedimentation path is of several $k_B T$ that typically covers the whole bulk phase diagram of the mixture. This allow us to neglect effects due to the finite height of the sample [22].

Each of the variables, a and s, is related to physical parameters of the system, the slope s is given by the ratio of the buoyant masses. The buoyant mass of species i is $m_i = (\rho_i - \rho_s)v_i$ where ρ_s is the solvent density, ρ_i is the mass density and v_i the particle volume. This will change by considering different size mixtures. For a binary mixture where both particles are made of the same material, s is given by:

$$s = \frac{v_2}{v_1} = \frac{\sigma_2^3}{\sigma_1^3} = \sigma^{*3} \tag{4.3}$$

The intercept a in addition to the dependence on s is related to the bulk chemical potentials μ_i^b.

The location of the path in the plane of chemical potentials is given by the bulk chemical potentials of the sample in the absence of gravity. Hence, the location is determined by the overall composition and concentration of the mixture. The stacking sequence observed in a sample follows directly from its

sedimentation path, since each time the sedimentation path crosses a boundary between two phases in the phase diagram, such as a binodal line, an interface appears in the vessel.

The set of all possible stacking sequences for a given bulk phase diagram forms the stacking diagram, a diagram with the variables a and s on its axes and with the boundaries between different stacking sequences represented. In Fig. 4.2 we show schematically a bulk phase diagram, a finite sedimentation path (corresponding to finite sample height) and examples of sedimentation paths that define boundaries in the stacking diagram. These boundaries are defined by the fact that at these points an infinitesimal change in s or a of the sedimentation path qualitatively changes the stacking sequence. There can be three different types of boundaries in the stacking diagram in the case of infinite sample height:

- **Sedimentation binodals:** formed by the set of all sedimentation paths that are tangent to a phase boundary (line (1) of Fig. 4.2) , e.g. binodal lines and percolation lines. The sedimentation paths that are tangent to the LV binodal are those that satisfy:

$$a_{LV}(s) = \mu_{2,LV}(\mu_1) - s\mu_1. \tag{4.4}$$

  Where $\mu_{2,LV}$ is the parameterization of the chemical potential of species 2 as a function of μ_1 at bulk LV coexistence. The slope, s, of the path is given by

$$s = \frac{d\mu_{2,LV}}{d\mu_1}. \tag{4.5}$$

- **Terminal lines:** Any sedimentation path that crosses an end point of a phase boundary (line (2) of Fig. 4.2), such as a critical point or a percolation end point, constitutes another boundary. Let $\mu_{i,end}$ be the chemical potential of species i at an end point of a phase boundary, then

$$a_{end}(s) = \mu_{2,end} - s\mu_{1,end}, \tag{4.6}$$

  describes all sedimentation paths that cross the end point. Equation (4.6) describes a line in the $a-s$ plane which we refer to as the terminal line.

- **Asymptotic terminal lines:** A bulk binodal may not terminate at finite chemical potentials (line (3) of Fig. 4.2), e.g. a binodal that represents a demixing region at high chemical potentials will tend also to an asymptote with a well defined slope:

$$\frac{\mu_{2,LV}}{\mu_{1,LV}} \to s_\infty. \tag{4.7}$$

  All paths with $s(a) = s_\infty$ define the sedimentation paths that are parallel to the asymptotic behaviour of a binodal.

Now we apply this theory to our case.

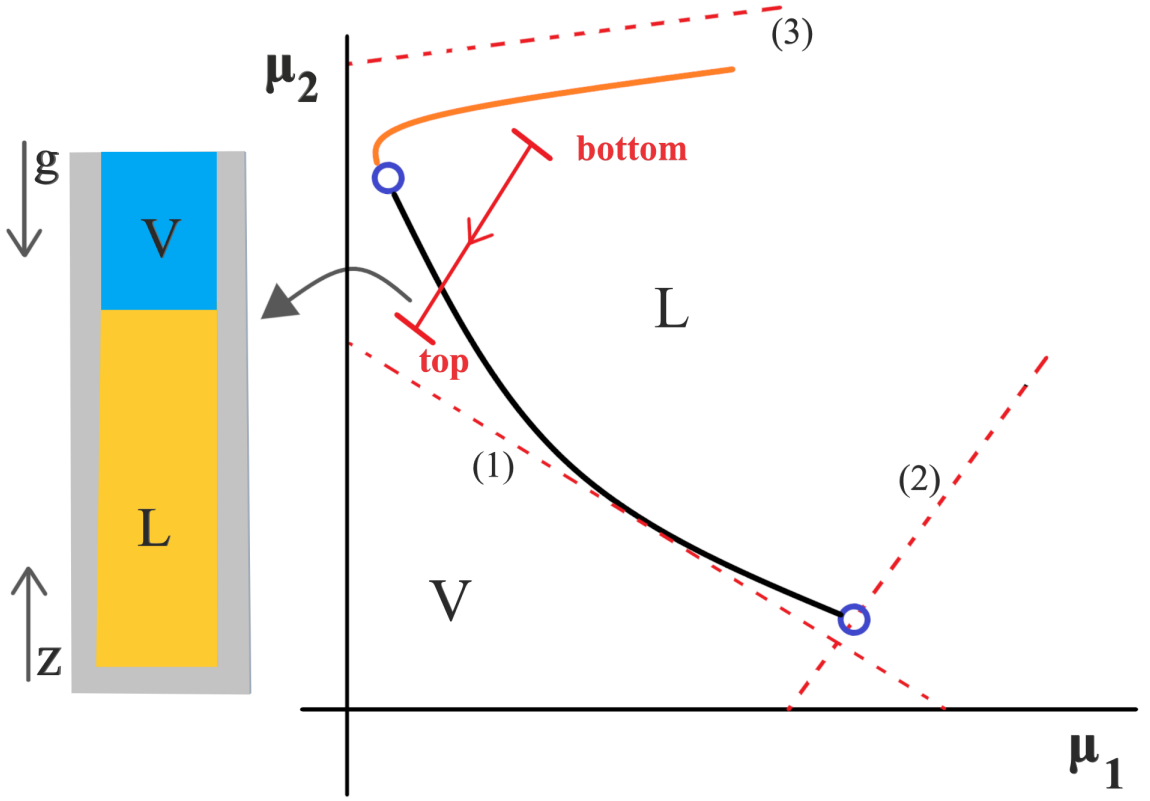

Figure 4.2: Schematic bulk phase diagram of a colloidal binary mixture in the plane of chemical potentials μ_1, μ_2. The black-solid line is a binodal where phases L and V coexist. The binodal ends at a critical point (empty blue circle) where a percolation line (orange-solid line) emerges. The solid-red line represents the sedimentation path of the mixture in a vessel of height h under gravity. The arrow indicates the direction of the path from the bottom to the top of the sample. The corresponding stacking sequence is bottom **L** and top **V**, as shown in the sketch. The dashed red lines are selected sedimentation paths for infinite height: (1) a path tangent to the binodal, (2) a path that crosses an ending point of a binodal, (3) a path parallel to the asymptotic behaviour of the percolation line.

4.2 The effect of gravity: Stacking diagram

In Fig. 4.3 we replot the chemical potential phase diagram and plot the corresponding stacking diagram for the simpler case of the closed miscibility gap, $T^* = 0.0718$ (Fig. 3.7(a)). The stacking diagram consists of a sedimentation binodal (formed by the paths tangent to the bulk binodal) and two terminal lines (formed by the paths that cross the critical point). These lines divide the stacking diagram in different regions. Each region corresponds to a qualitatively different stacking sequence. The stacking sequence of each region can be found by selecting a point in the region of interest and plotting the corresponding sedimentation path in the bulk phase diagram. As an example we plot two points in the stacking diagram and the corresponding sedimentation paths in the phase diagram. The stacking sequences are named from bottom to top of the sample, i.e. the stacking sequence **LV** forms a liquid phase in the bottom of the sample and a vapor phase in the top (the opposite happens for the stacking sequence **VL**). Although there are only two stable phases in the bulk system, (**L**,**V**), the stacking diagram contains up to five different stacking sequences. The stacking sequence **VLV** can be obtained for a very small range of values.

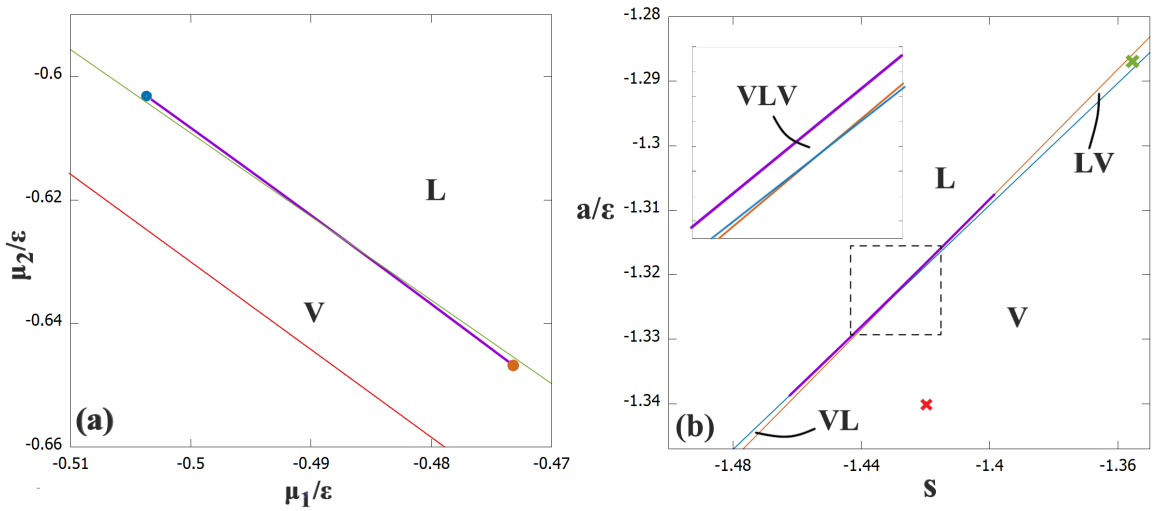

Figure 4.3: (a) Chemical potential phase diagram and (b) corresponding stacking diagram for the temperature $T^* = 0.0718$. (a) The binodal is represented by the violet line, critical points are the blue and brown points, the green and red lines are examples of sedimentation paths corresponding to the stacking sequences **LV** and **V** respectively. (b) The violet line is the sedimentation binodal and blue and brown lines are the terminal lines of the critical points, each region defining a qualitatively different stacking sequence described by the bold text. The points in green and red are the paths represented in (a).

Next, we do the same for the more complex case of two coexistence regions ($T^* = 0.065$), (Fig. 3.7(b)). We replot the μ_2 vs μ_1 diagram Fig. 4.4(a) and plot the corresponding stacking diagram Fig. 4.4(b). The stacking diagram consists of three sedimentation binodals (one corresponding to the bulk binodal and two others to the percolation lines), four terminal lines (two for the critical points and two for the percolation end points) and two asymptotic terminal lines corresponding to the asymptotic behavior of the percolation lines. Stacking sequences defined by the same type of boundaries are equivalent. This is because we have not differentiated between the vapor phase rich in 2A particles and the one rich in 3B particles. Nevertheless, the stacking diagram is quite rich, with stacking sequences with up to five phases in the region surrounding the sedimentation binodals as is shown by the zoom of Fig. 4.4). Two sedimentation paths are plotted as examples. The regions between the 4 terminal lines are not defined and the difference between equivalent stacking sequences is made below.

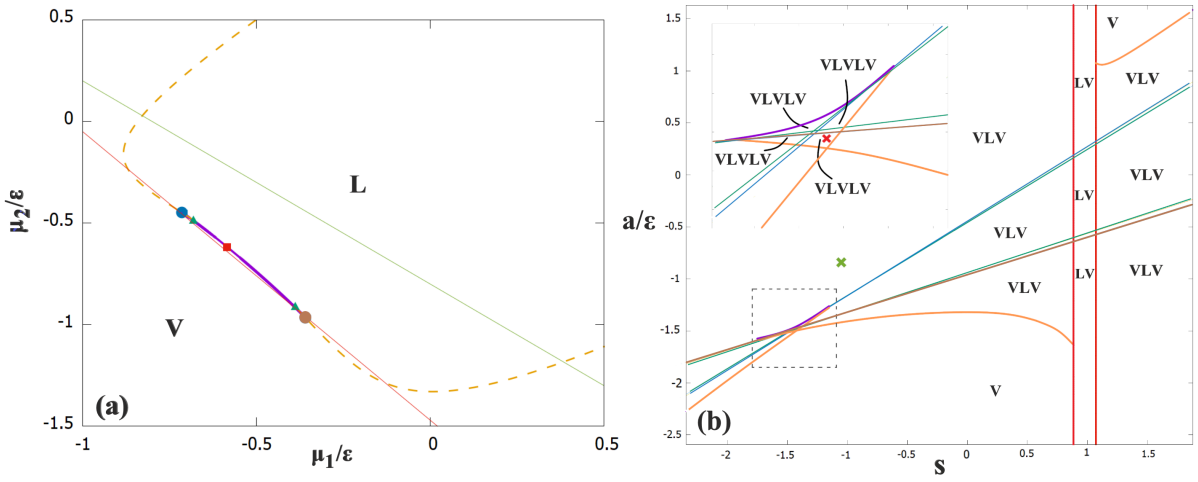

Figure 4.4: (a) Chemical potential phase diagram and (b) corresponding stacking diagram for the temperature $T^* = 0.065$. (a) The binodal is represented by the violet line, the percolation lines are the orange dashed lines. Critical points are the blue and brown points, the azeotropic point is the red square and the green and red lines are examples of sedimentation paths corresponding to the stacking sequences **VLV** and **VLVLV** respectively. (b) The violet line is the sedimentation binodal, the orange lines are the percolation sedimentation binodals. Blue lines are the terminal lines corresponding to the critical points and green lines are the terminal lines corresponding to the percolation end points. Red vertical lines are the asymptotic terminal lines of the percolation lines. The points in green and red are the ones represented in (a).

It is informative to divide the phases V_1 and V_2; the vapor phases reached mostly with species 1 and 2 respectively. By doing so, the percolation lines are easily distinguishable and the abundance of each particle species over the other is specified. In Fig. 4.5 we replot the chemical potential diagram for $T^* = 0.065$ but this time displaying the different phases. Also, because the percolation lines approach the binodal from the vapor phase (see zoom of Fig. 4.5) we also define V_1' and V_2', the vapor percolated phases. This helps to interpret the equivalent stacking sequences in the stacking diagram. In Fig. 4.6 we replot the stacking diagram for $T* = 0.065$ with the phases V_1 and V_2 differentiated. By doing so, we obtain an even richer diagram, with over 20 different stacking sequences. The regions between the 4 terminal lines are only possible for a small range of values, nevertheless their difference from the neighbouring regions is the crossing of one of the vapor percolated regions, V_1' or V_2'.

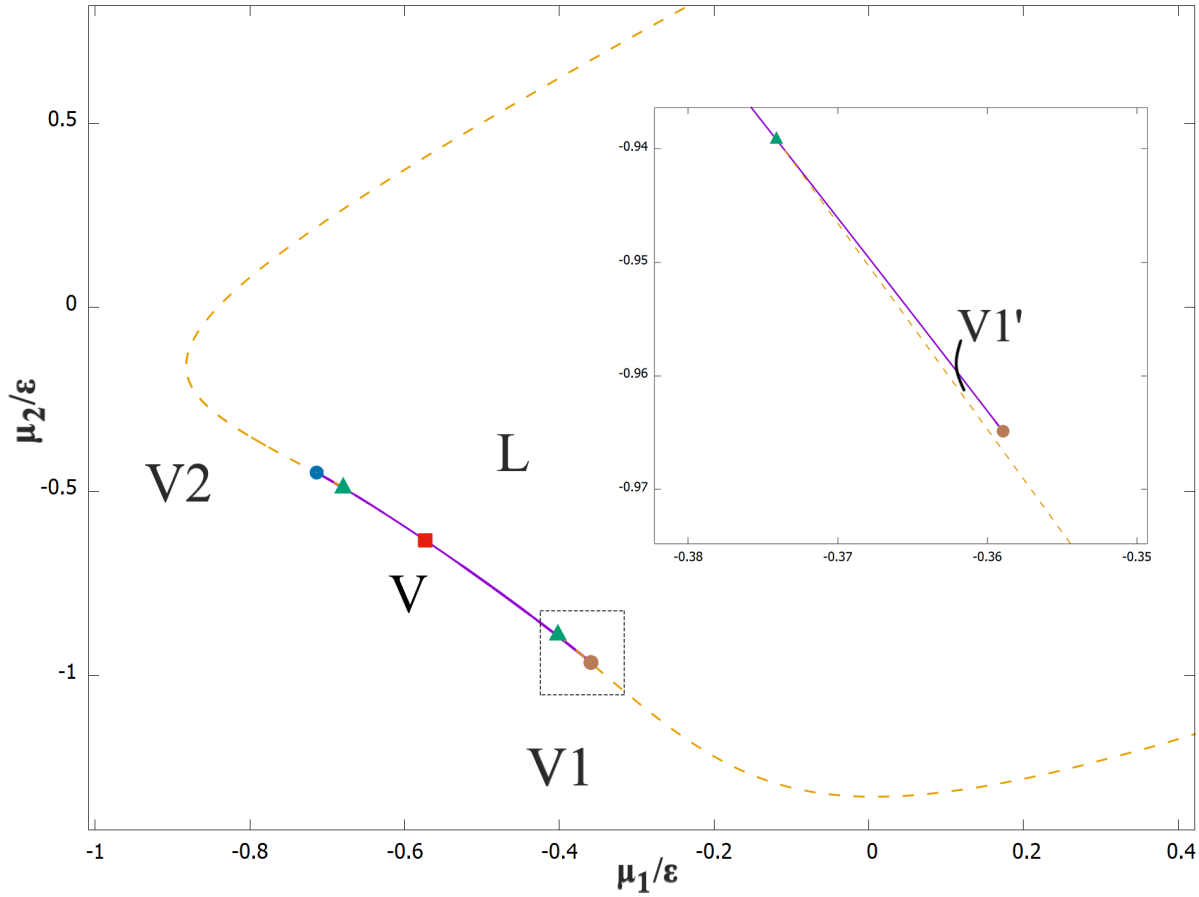

Figure 4.5: Phase diagram in the chemical potential plane. We define phases **V1** the vapor phase reached mostly with species 1 and **V2** the vapor phase reached mostly with species 2. From the zoom we can see that the percolation lines approach the binodal from the vapor phase this is why we also define **V1'** (not pictured) and **V2'** the percolated vapor phases.

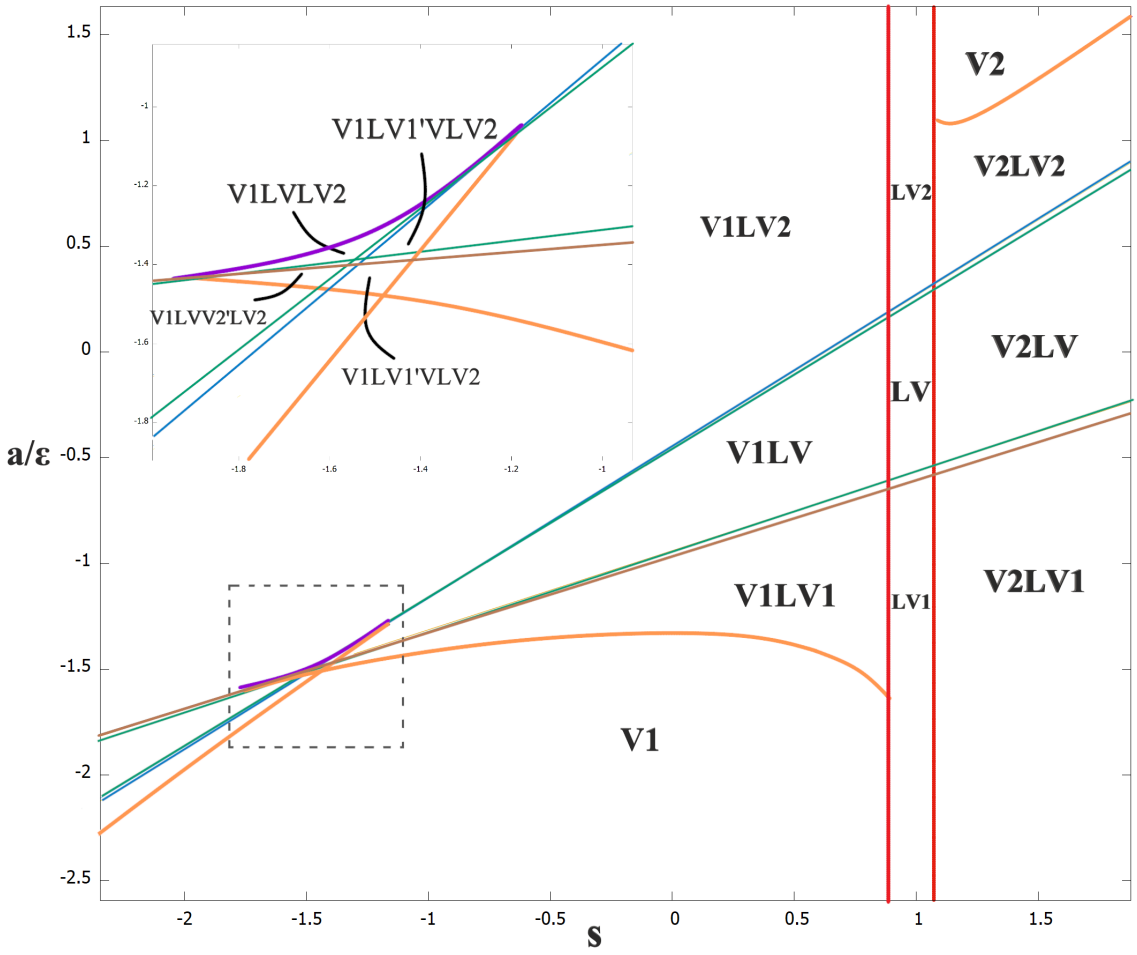

Figure 4.6: Stacking diagram showing some of the main stacking sequences when distinguishing between the vapor phase rich in 2A and the one rich in 3B. The violet line is the sedimentation binodal of the bulk binodal. The orange lines correspond to the sedimentation binodals of the percolation lines. The blue and green lines are the terminal lines corresponding to the critical points and the percolation end points respectively. The red lines are the asymptotic terminal lines of the percolation lines

4.3 Sedimentation for different sized mixtures

In section **3.2** the phase diagrams obtained for different size mixtures showed the same topologies as those for the case of equal sized mixtures. Hence, the stacking diagrams of different sized mixtures are roughly the same as the two previous cases. Since we have the same number and type of phase boundaries. Nevertheless, we study if a stacking sequence can change by only changing the size of the particles. To do so, we compare stacking diagrams of equal and different sized mixtures (corresponding to phase diagrams with the same topology).

We consider a sedimentation path in the case of equal-sized particles (a point in the stacking diagram) and map it out to the different sized mixture case. Considering that the particles are made of the same material, we transform the parameter s to (see Eq.4.3)

$$s' = (v_2'/v_1')s = \sigma^{*3}s, \tag{4.8}$$

where v_i' is the volume of particles of species i after the transformation. The parameter $a = \mu_2^b - s\mu_1^b$ will transform by this change and also by the change in the corresponding chemical potentials, i.e. chemical

potentials at equal pressures

$$\mu_i'^b\Big|_p = \mu_i^b\Big|_p, \tag{4.9}$$

$a' = \mu_2'^b - s'\mu_1'^b$ (another possibility would be to compare two samples with the same densities in both systems). In Fig. 4.7 two chemical potential diagrams and the corresponding stacking diagrams are shown, one corresponding to the equal sized mixture ($\sigma^* = 1$) and the other corresponding to the different sized mixture $\sigma^* = 1.3$. Although they are similar, we can see through the point (and sedimentation path) plotted, that it is possible to have different stacking sequences just by changing the size of the particles. In general, this is possible for points in the stacking diagram that are close to boundaries between different stacking sequences. It is also easier to reach different stacking sequences if the μ_1 vs μ_2 diagrams are not too similar to each other which means that by considering a big difference in the sizes of the particles the number of paths that change will increase. This is not surprising since for $\sigma^* > 1.63$ the topology of the phase diagram changes. This means there will be stacking sequences for one system that are impossible to obtain for the other.

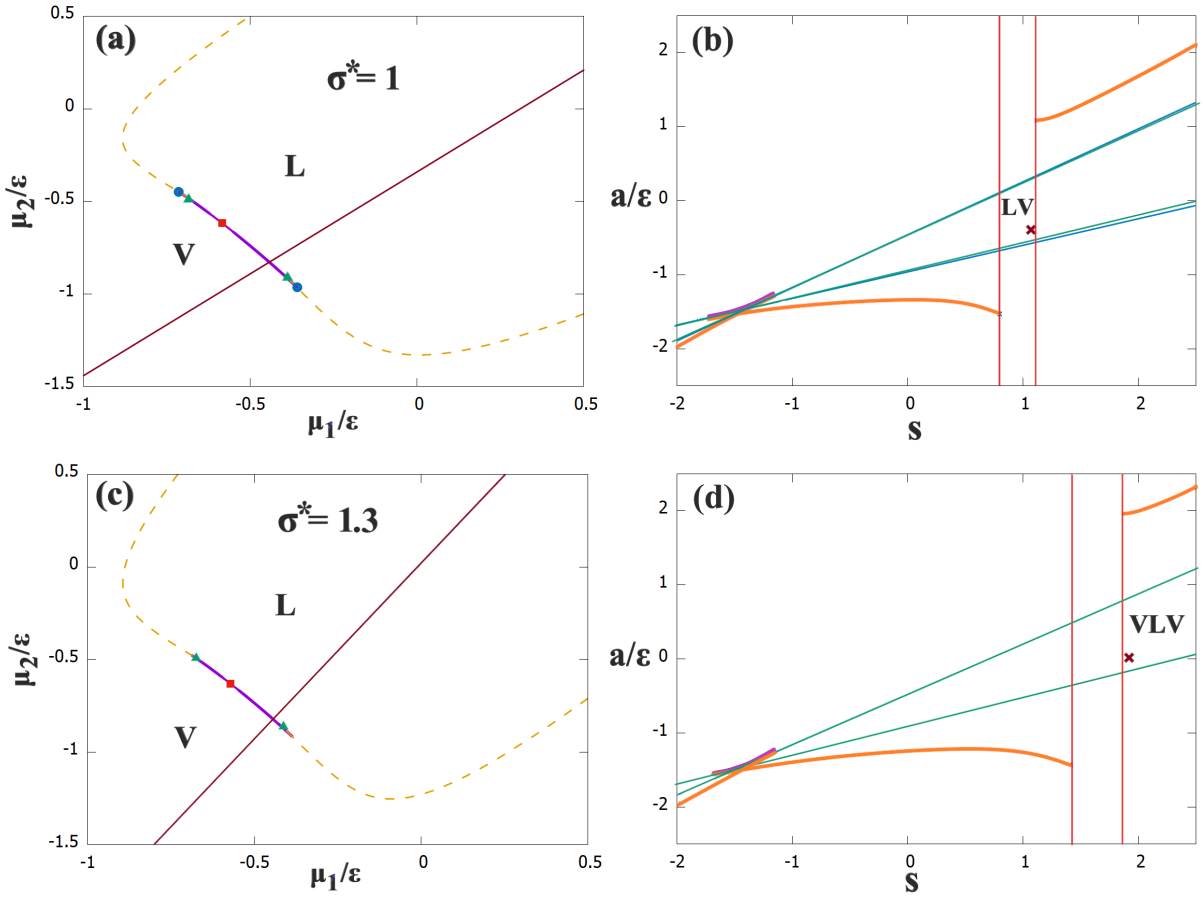

Figure 4.7: Comparison of two phase diagrams and corresponding stacking diagrams. (a) and (c) are chemical potential phase diagrams corresponding to the cases $\sigma_B/\sigma_A = 1$ and $\sigma_B/\sigma_A = 1.3$, the sedimentation path in dark red corresponds to **LV** in the equal size mixture and to **VLV** in the different sized mixture (the path crosses the percolation lines for higher values of μ_2). (b) and (d) are the corresponding stacking diagram for the cases $\sigma_B/\sigma_A = 1$ and $\sigma_B/\sigma_A = 1.3$ respectively. The dark red cross is the point which was mapped from the equal to the different sized mixture; the fact that they define different stacking sequences means that just by changing the size of the particles we can have different stacking sequences.

Chapter 5

Conclusion

We have investigated the phase behavior of a binary mixture of patchy colloids. In particular we have studied the case where one species had 2 patches and the other 3 patches (2A-3B). We considered only inter-species bonding, meaning that only particles of different species could bond to each other. This defines an energy scale that allows to control the extension of bonds using the composition of both species. First we have studied the phase diagrams of the equal sized system. Two topologies are possible, depending on the values of temperature and pressure: one with two coexistence regions (one rich in 2A particles and another in 3B) with lower critical points and an azeotropic point, and a second topology which consists of a closed miscibility gap with upper and lower critical points. These diagrams were displayed in different representations: pressure-composition, temperature-composition and chemical potential planes. Percolation lines show that the vapor phase can percolate and that the liquid phases are always percolated. The analysis of the critical properties shows that the empty fluid regime is never reached and the phase richer in 3B forms bigger clusters than the phase rich in 2A. All critical properties of the system tend to an asymptotic value as the temperature vanishes.

Next, we have investigated different sized mixtures. Changing the relative size of the particles does not change the topologies of the phase diagram already studied, but mimics the effect of increasing the temperature or the pressure, i.e. the coexistence regions shrink by increasing the relative difference of sizes. The change in size has no effect on the percolation lines. This is because there is a compensation effect of the bonding probabilities, i.e. while the probability of having bonded patches of one type increases, the probability of the other type decreases. This helps to understand the fact that by increasing $\sigma^* = \sigma_A/\sigma_B$ the average size of the clusters of the phase rich in 3B decreases and the rich in 2A increases ($(1-X_A)$ increases and $(1-X_B)$ decreases).

We have also investigated the effect of gravity. The stacking diagrams were calculated in the limit of very high (infinite) sample heights. For the single coexistence region diagram, five different stacking sequences occur while for the two coexistence region diagram, a much richer stacking diagram was obtained, with more than twenty stacking sequences.

Considering the fact that different sized mixtures do not impose new topologies to the phase diagrams means the phase stacking phenomenology possible to obtain in both systems is similar. Therefore, when considering different sized mixtures, we have focused our attention on mapping sedimentation paths in the equal sized system to the different sized case. We have discovered that just by changing the size of the particles we are able to obtain different stacking sequences. This work is a first step towards understanding the effect of changing the relative size of the particles on the phase behavior of patchy colloids. Further research considering different functionalities and more energy scales would enrich and help generalize our results. The systematization of the effect of changing the relative size of the

particles on the stacking diagram is of interest to predict how we can control the sedimentation-diffusion equilibrium. We conclude by saying that our work could be further developed to help determine the maximum uncertainty possible in the fabrication of colloidal particles of each particular system, since we were able to study how much the relative size of the particles could change without changing the topology of the phase diagram (or the phase stacking phenomenology).

Chapter 6

Appendices

6.1 Free energy of an ideal gas mixture

The hamiltonian for a classical canonical ensemble (mechanical system in thermal equilibrium with a heat bath at a fixed temperature) of a one component ideal gas composed of N particles is [2]

$$H = \sum_{i=1}^{N} \frac{p_i^2}{2m}, \tag{6.1}$$

where p_i is the linear momentum of each particle and m the mass of the particles. The partition function is

$$Z(T,V) = \int \frac{d^{3N}pd^{3N}q}{N!h^{3N}} e^{-\beta(p_1^2+\ldots+p_N^2)/2m} = \frac{V^N}{N!}\Big(\int_{-\infty}^{+\infty} \frac{dp}{h} e^{-\beta p^2/2m}\Big)^{3N}, \tag{6.2}$$

where V is the volume of the system, the last integral is a gaussian integral exactly soluble: $\int_{-\infty}^{\infty} e^{-a(x)^2}\,dx = \sqrt{\frac{\pi}{a}}$, with $a = \beta/2m$. Our partition function then becomes

$$Z(T,V) = \frac{1}{N!}\frac{V}{\lambda^3}, \tag{6.3}$$

where $\lambda = h/\sqrt{2\pi m k_B T}$ is the de Broglie thermal wavelength. This result can be generalized to a mixture of i ideal gases, in this case the partition function is simply the multiplication of the partition function of each component since the gases are noninteracting, i.e. the energy of each molecule is independent of the other molecules:

$$Z(T,V) = \prod_{i=1}^{i} \frac{1}{N_i!}\frac{V}{\lambda_i^3} \tag{6.4}$$

The Helmholtz free energy is written from the partition function as

$$F = -k_B T \ln(Z) = -k_B T \sum_{i=1}^{i} \ln\Big(\frac{1}{N_i!}\frac{V}{\lambda_i^3}\Big), \tag{6.5}$$

Using the Stirling approximation $lnN! \approx NlnN - N$ this becomes

$$F \approx k_B T \sum_i [N_i(\ln \rho_i \lambda_i^3 - 1)] \tag{6.6}$$

Where $\rho_i = N_i/V$ is the number density of each species. For a binary mixture, the Helmholtz free energy per particle is

$$f = F/N = k_B T \sum_{i=1}^{2} x_i[\ln(x_i \rho \lambda_i^3)] \tag{6.7}$$

Where x_i are the different fractions of particles, $x_i = N_i/N$, this reduces to

$$\beta f = x_1[\ln \rho x_1 \lambda_1^3 - 1] + x_2[\ln \rho x_2 \lambda_2^3 - 1] = (x_1 + x_2)[\ln \rho - 1] + x_1 \ln(x_1 \lambda_1) + x_2 \ln(x_2 \lambda_2) \tag{6.8}$$

Since $x_1 + x_2 = 1$ we can write

$$\beta f = \ln(\rho) - 1 + \sum_{i=1,2} x_i \ln(x_i \lambda_i) \tag{6.9}$$

This is term by term Eq.2.7.

6.2 Calculation of the excess free energy

Let us consider a binary mixture with N_i particles of species $i = 1, 2$. The pressure can be calculated from the free energy:

$$p = -\left(\frac{\partial F}{\partial V}\right)_{N_1, N_2, T}, \tag{6.10}$$

by integrating this expression we can calculate the free energy:

$$F(V, N_1, N_2, T) = F(V_0, N_1, N_2, T) - \int_{V_0}^{V} p dV. \tag{6.11}$$

Here, V_0 is an arbitrary volume. This is a general equality. In what follows $F(V, N_1, N_2, T)$ is the free energy of the system under study minus the bonding part. In [35] the compressibility factor Z_{eCS-II} is given,

$$\beta p \equiv \frac{N_1 + N_2}{V} Z_{eCS-II}(\eta, N_1, N_2; \sigma_1, \sigma_2), \tag{6.12}$$

as a function of σ_i, the diameter of particles of species i, $\eta = \frac{\pi}{6} \sum_i N_i \sigma_i^3 / V$ the total packing fraction and the temperature, T. Replacing p by Z_{eCS-II} in 6.11 using 6.12 we obtain

$$\beta f(V, N_1, N_2, T) = \beta f(V_0, N_1, N_2, V) - \int_{V_0}^{V} Z_{eCS-II}(\eta, N_1, N_2; \sigma_1, \sigma_2) \frac{dV}{V}, \tag{6.13}$$

where f is the free energy per particle. Therefore, we obtain the free energy per particle of a system by integrating the compressibility factor. From Santos paper [35] (eq. 22 and 23) this is:

$$Z_{eCS-II}(\eta) = \frac{1}{1-\eta} + \frac{3\eta C_1}{(1-\eta)^2} + \frac{\eta^2(3-\eta)C_2}{(1-\eta)^3} - \frac{\eta^3 C_3}{(1-\eta)^2} \tag{6.14}$$

The integral in 6.13 can be simplified:

$$-\int_{V_0}^{V} Z_{eCS-II}(\eta, N_1, N_2; \sigma_1, \sigma_2) \frac{dV}{V} = \int_{\eta_0}^{\eta} Z_{eCS-II}(\eta, N_1, N_2; \sigma_1, \sigma_2) \frac{d\eta}{\eta} \tag{6.15}$$

And performing this integral for the compressibility factor 6.14 taking into account the fact that this still contains the ideal contribution leads to the expression for the free energy in Eq.2.8.

Bibliography

[1] L. P. Kadanoff. *Theories of Matter: Infinities and Renormalization*. 2013. DOI: 10.1093/oxfordhb/9780195392043.013.0005.

[2] K. Huang. *Introduction to Statistical Physics*. Chapman and Hall/CRC; 2 edition, 2009. DOI: 10.1201/9781439878132.

[3] H. Nishimori and G. Ortiz. *Elements of Phase Transitions and Critical Phenomena*. Oxford University Press, 2015. DOI: 10.1093/acprof:oso/9780199577224.001.0001.

[4] R. Piazza. *Soft Matter: the stuff that dreams are made of*. Springer-Verlag Italia, 2010. DOI: 10.1007/978-94-007-0585-2.

[5] C. E. Reese, C. D. Guerrero, J. M. Weissman, K. Lee and S. A. Asher. "Synthesis of Highly Charged, Monodisperse Polystyrene Colloidal Particles for the Fabrication of Photonic Crystals". In: *Journal of Colloid and Interface Science* 232.1 (2000), pp. 76–80. DOI: 10.1006/jcis.2000.7190.

[6] S. J. Sagou, S. S. Kouassi, and F. Thomas. "Influence of Metallic Ions on the Aggregation of Soft Colloidal Polysaccharides". In: *Journal of Colloid and Interface Science* 5.2 (2017), pp. 23–30. DOI: 10.11648/j.sjc.20170502.

[7] I. I. Slowing , J.-P. L. Vivero-Escoto, C.-W. Wu and V. S.-Y. Lin. "Mesoporous silica nanoparticles as controlled release drug delivery and gene transfection carriers". In: *Advanced Drug Delivery Reviews* 60.11 (2008), pp. 1278–1288. DOI: 10.1016/j.addr.2008.03.012.

[8] H. Liu, S. K. Kumar, and F. Sciortino. "Vapor-liquid coexistence of patchy models: Relevance to protein phase behavior". In: *The Journal of Chemical Physics* 127.8 (2007), p. 084902. DOI: 10.1063/1.2768056.

[9] Yufeng W., Yu W., D. R. Breed, V. N. Manoharan, L. Feng, A. D. Hollingsworth, M. Weck and D. J. Pine. "Colloids with valence and specific directional bonding". In: *Nature* 491 (2012), pp. 51–55. DOI: 10.1038/nature11564.

[10] P.I.C. Teixeira and J. M. Tavares. "Phase behaviour of pure and mixed patchy colloids - Theory and simulation". In: *Current Opinion in Colloid Interface Science* 30 (2017), pp. 16–24. DOI: 10.1016/j.cocis.2017.03.01.

[11] E. Bianchi, J. Largo, P. Tartaglia , E. Zaccarelli and F. Sciortino. "Phase Diagram of Patchy Colloids: Towards Empty Liquids". In: *Phys. Rev. Lett.* 97 (16 2006). DOI: 10.1103/PhysRevLett.97.168301.

[12] J. Russo, J. M. Tavares, P. I. C. Teixeira, M. M. Telo da Gama and F. Sciortino. "Reentrant Phase Diagram of Network Fluids". In: *Phys. Rev. Lett.* 106.8 (), p. 085703. DOI: 10.1103/PhysRevLett.106.085703.

[13] L. Rovigatti, J. Maria Tavares, and F. Sciortino. “Self-Assembly in Chains, Rings, and Branches: A Single Component System with Two Critical Points”. In: *Phys. Rev. Lett.* 111 (16 2013), p. 168302. DOI: 10.1103/PhysRevLett.111.168302.

[14] W. R. Smith and I. Nezbeda. “A simple model for associated fluids”. In: *The Journal of Chemical Physics* 81.8 (1984), pp. 3694–3699. DOI: 10.1063/1.448120.

[15] A. Lomakin, N. Asherie, and G. B. Benedek. “Aeolotopic interactions of globular proteins”. In: *Proceedings of the National Academy of Sciences* 96.17 (1999), pp. 9465–9468. DOI: 10.1073/pnas.96.17.9465.

[16] G.-R. Yi, D. J. Pine, and S. Sacanna. “Recent progress on patchy colloids and their self-assembly”. In: *Journal of Physics: Condensed Matter* 25.19 (2013), p. 193101. DOI: 10.1088/0953-8984/25/19/193101.

[17] D. de las Heras, J. M. Tavares, and M. Telo da Gama. “Phase diagrams of binary mixtures of patchy colloids with distinct numbers and types of patches: The empty fluid regime”. In: *J. Chem. Phys.* 134.104904 (2011). DOI: 10.1063/1.3561396.

[18] D. de las Heras, J. M. Tavares, and M. Telo da Gama. “Phase diagrams of binary mixtures of patchy colloids with distinct numbers of patches: the network fluid regime”. In: *Soft Matter* 7.5615 (2011). DOI: 10.1039/C0SM01493A.

[19] S. Biffi, R. Cerbino, F. Bomboi, E. M. Paraboschi, R. Asselta, F. Sciortino and T. Bellini. “Phase behavior and critical activated dynamics of limited-valence DNA nanostars”. In: *Proceedings of the National Academy of Sciences* 110.39 (2013), pp. 15633–15637. DOI: 10.1073/pnas.1304632110.

[20] D. de las Heras and M. Schmidt. “Sedimentation stacking diagram of binary colloidal mixtures and bulk phases in the plane of chemical potentials”. In: *J. Phys.: Condens. Matter* 27.194115 (2015). DOI: 10.1088/0953-8984/27/19/194115.

[21] R. Piazza. “Settled and unsettled issues in particle settling”. In: *Reports on Progress in Physics* 77.5 (2014), p. 056602. DOI: 10.1088/0034-4885/77/5/056602.

[22] D. de las Heras, N. Doshi, T. Cosgrove, J. Phipps, D. I. Gittins, J. S. van Duijneveldt and M. Schmidt. “Floating nematic phase in colloidal platelet-sphere mixtures”. In: *Scientific Reports* 2.1 (2012), p. 789. DOI: 10.1038/srep00789.

[23] D. de las Heras and M. Schmidt. “The phase stacking diagram of colloidal mixtures under gravity”. In: *Soft Matter* 9 (36 2013), pp. 8636–8641. DOI: 10.1039/C3SM51491A.

[24] D. de las Heras, L. L. Treffenstädt, and M. Schmidt. “Reentrant network formation in patchy colloidal mixtures under gravity”. In: *Phys. Rev. E* 93 (3 2016), p. 030601. DOI: 10.1103/PhysRevE.93.030601.

[25] T. Geigenfeind and D. de las Heras. “The role of sample height in the stacking diagram of colloidal mixtures under gravity”. In: *Journal of Physics: Condensed Matter* 29.6 (2016), p. 064006. DOI: 10.1088/1361-648x/aa4e04.

[26] R. Fantoni and G. Pastore. “Wertheim and Bjerrum-Tani-Henderson theories for associating fluids: A critical assessment”. In: *The Journal of Chemical Physics* 141.7 (2014), p. 074108. DOI: 10.1063/1.4892878.

[27] W. G. Chapman, G. Jackson, and K. E. Gubbins. “Phase equilibria of associating fluids”. In: *Molecular Physics* 65.5 (1988), pp. 1057–1079. DOI: 10.1080/00268978800101601.

[28] M. S. Wertheim. “Fluids of dimerizing hard spheres, and fluid mixtures of hard spheres and dispheres”. In: *The Journal of Chemical Physics* 85.5 (1986), pp. 2929–2936. DOI: 10.1063/1.451002.

[29] W. Bol. “Monte Carlo simulations of fluid systems of waterlike molecules”. In: *Molecular Physics* 45.3 (1982), pp. 605–616. DOI: 10.1080/00268978200100461.

[30] N. Kern and D. Frenkel. “Fluid–fluid coexistence in colloidal systems with short-ranged strongly directional attraction”. In: *The Journal of Chemical Physics* 118.21 (2003), pp. 9882–9889. DOI: 10.1063/1.1569473.

[31] M.S. Wertheim. “Fluids with highly directional attractive forces. I. Statistical thermodynamics”. In: *J Stat Phys* 35.19–34 (1984). DOI: 10.1007/BF01017362.

[32] J.S. Rowlinson and F. L. Swinton. *Liquid and Liquid mixtures*. Butterworth-Heinemann, 1982.

[33] J. P. Hansen and I.R. McDonald. *Theory of Simple Liquids: with Applications to Soft Matter*. Academic Press; 4 edition, 2013. DOI: 10.1016/C2010-0-66723-X.

[34] Y. V. Kalyuzhnyi, B. D. Marshall, W. G. Chapman and P. T. Cummings. “Second-order resummed thermodynamic perturbation theory for central-force associating potential: Multi-patch colloidal models”. In: *The Journal of Chemical Physics* 139.4 (2013), p. 044909. DOI: 10.1063/1.4816128.

[35] A. Santos, S. B. Yuste, and M. L. de Haro. “Contact values of the radial distribution functions of additive hard-sphere mixtures in d dimensions: A new proposal”. In: *The journal of Chemical Physics* 117.5785 (2002). DOI: 10.1063/1.1502247.

[36] Masao D. *Soft Matter Physics*. Oxford University press, 2013. DOI: 10.1093/acprof:oso/9780199652952.001.0001.

[37] J. S. Rowlinson and F. L. Swinton. “Chapter 4 - The thermodynamics of liquid mixtures”. In: *Liquids and Liquid Mixtures*. Third Edition. 1982, pp. 86–131. DOI: 10.1016/B978-0-408-24193-9.50008-4.

[38] M.S. Wertheim. “Fluids with highly directional attractive forces. IV. Equilibrium polymerization”. In: *Journal of Statistical Physics* 42.3 (1986), pp. 477–492. DOI: 10.1007/BF01127722.

[39] P. J. Flory. “Molecular Size Distribution in Three Dimensional Polymers. I. Gelation1”. In: *Journal of the American Chemical Society* 63.11 (1941), pp. 3083–3090. DOI: 10.1021/ja01856a061.

[40] W. H. Stockmayer. “Theory of Molecular Size Distribution and Gel Formation in Branched-Chain Polymers”. In: *The Journal of Chemical Physics* 11.2 (1943), pp. 45–55. DOI: 10.1063/1.1723803.

[41] J. M. Tavares, P. I. C. Teixeira, and M. M. Telo da Gama. “Percolation of colloids with distinct interaction sites”. In: *Phys. Rev. E* 81.010501(R) (2010). DOI: 10.1103/PhysRevE.81.010501.

[42] P. H. van Konynenburg, R. L. Scott, and J. S. Rowlinson. “Critical lines and phase equilibria in binary van der Waals mixtures”. In: *Philosophical Transactions of the Royal Society of London. Series A, Mathematical and Physical Sciences* 298.1442 (1980), pp. 495–540. DOI: 10.1098/rsta.1980.0266.

[43] J. Perrin. *Atoms*. Constable Co, 1916. DOI: 10.1038/099044b0.

[44] R. Piazza, T. Bellini, and V. Degiorgio. “Equilibrium sedimentation profiles of screened charged colloids: A test of the hard-sphere equation of state”. In: *Phys. Rev. Lett.* 71 (25 1993), pp. 4267–4270. DOI: 10.1103/PhysRevLett.71.4267.